

3-22-2012

Probabilistic Model for Laser Damage to the Human Retina

David R. Wooddell

Follow this and additional works at: <https://scholar.afit.edu/etd>

Part of the [Occupational Health and Industrial Hygiene Commons](#)

Recommended Citation

Wooddell, David R., "Probabilistic Model for Laser Damage to the Human Retina" (2012). *Theses and Dissertations*. 1248.
<https://scholar.afit.edu/etd/1248>

This Thesis is brought to you for free and open access by the Student Graduate Works at AFIT Scholar. It has been accepted for inclusion in Theses and Dissertations by an authorized administrator of AFIT Scholar. For more information, please contact richard.mansfield@afit.edu.



PROBABILISTIC MODEL FOR LASER DAMAGE TO THE HUMAN RETINA

THESIS

David Alan Wooddell, Jr., Captain, USAF

AFIT-OR-MS-ENS-12-30

DEPARTMENT OF THE AIR FORCE

AIR UNIVERSITY

AIR FORCE INSTITUTE OF TECHNOLOGY

Wright-Patterson Air Force Base, Ohio

Distribution Statement A
APPROVED FOR PUBLIC RELEASE; DISTRIBUTION UNLIMITED

The views expressed in this thesis are those of the author and do not reflect the official policy or position of the United States Air Force, Department of Defense, or the United States Government. This material is declared a work of the U.S. Government and is not subject to copyright protection in the United States.

AFIT-OR-MS-ENS-12-30

PROBABILISTIC MODEL FOR LASER DAMAGE TO THE
HUMAN RETINA

THESIS

Presented to the Faculty of the
Department of Operational Sciences
Graduate School of Engineering and Management
Air Force Institute of Technology
Air University
Air Education and Training Command
in Partial Fulfillment of the Requirements for the
Degree of Master of Operations Research

David Alan Wooddell, Jr., B.S.
Captain, USAF

March, 2012

Distribution Statement A
APPROVED FOR PUBLIC RELEASE; DISTRIBUTION UNLIMITED

PROBABILISTIC MODEL FOR LASER DAMAGE TO THE
HUMAN RETINA

David Alan Wooddell, Jr., B.S.
Captain, USAF

Approved:

 //SIGNED//

Dr. Raymond Hill,
Thesis Advisor

18 March 2012

Date

 //SIGNED//

Dr. Christine Schubert-Kabban
Reader

18 March 2012

Date

Abstract

The proliferation of laser systems in the 21st-century is fueled by an increasing demand and comprehension of the capabilities they provide. Understanding how lasers interact with media during propagation is a premiere field of physics. The subject area known as laser bioeffects explores laser interactions with biological cells, tissues, organs, and bodies. This research includes laser applications used in medicine, establishes safe exposure limits for industry and academia, and generally studies the many effects of laser light on living creatures. The bioeffects community relies heavily on deterministic modeling and simulation tools to support experimental research into damage thresholds and laser effects. However, recent laser applications require a probabilistic approach to support risk management and analyses methodologies. Some probabilistic models exist but their assumptions are largely biased due to sampling and reporting techniques. This research focuses on building the first-ever population based probabilistic model for retinal damage using a statistical model of the optical properties and dimensions of the human eye. Simulated population distributions are used as input to propagation and thermal damage models for analysis. The results of this research are intended to provide a foundation for future probabilistic models and applications.

Acknowledgements

Although I am credited with authorship of this document, it wouldn't have been possible without the contributions of many others. First, I must give thanks to the Lord for His grace in giving me the wisdom and His ear when I needed it. Second, I must thank my wife for being so much more than I deserve. She supported me throughout my research, was a wonderful mother, and carried a 4.0 GPA in her own full-time college work. I am also thankful for my son and daughter and dedicate this work and all I do to make their world a better place.

I would like to thank my advisor, Dr. Raymond Hill, for his guidance and trust in my ability. His support and direction, as well as his encouragement to keep family first, made this effort possible. A special thanks also goes to Dr. Christine Schubert-Kabban for her direction in the area of biostatistics.

Additionally, this work would not have been possible without the true mentorship of Dr. Robert J. Thomas. His guidance and support since 2007 has allowed me to establish my research in a relevant area. He is truly dedicated to the directed energy bioeffects community and works tirelessly as a leader and pioneer in laser bioeffects research.

Finally, Dr. Benjamin Rockwell, Dr. Jos Rozema, Dr. C. D. Clark, III, Mr. Gary Noojin, Dr. James Stringham, my peers in GOR12M, and my instructors at the Air Force Institute of Technology deserve acknowledgement for their significant involvement in some aspect of this research.

David Alan Wooddell, Jr.

Table of Contents

	Page
Abstract	iv
Acknowledgements	v
List of Figures	ix
List of Tables	xii
List of Abbreviations	xiii
1. Introduction	1-1
2. Background	2-1
3. An Analysis of the Influences of Biological Variance, Measurement Error, and Uncertainty on Retinal Photothermal Damage Threshold Studies	3-1
3.1 Abstract	3-1
3.2 Introduction	3-1
3.3 Background	3-2
3.4 Method	3-12
3.5 Results	3-18
3.6 Discussion	3-22
3.7 Conclusion	3-24
4. Biological Variance-Based Dose Response Model for 514 to 1064 Nanometer Laser Exposures	4-1
4.1 Abstract	4-1
4.2 Introduction	4-1

	Page
4.3 Background	4-3
4.4 Method	4-11
4.4.1 Estimating Dose for Probability of Damage	4-16
4.4.2 Estimating Probability of Damage for Dose	4-17
4.5 Results	4-18
4.5.1 Trade Space for 532-nm Dazzler Systems	4-19
4.5.2 Collateral Risk Estimates for 1064-nm Emitter	4-20
4.6 Conclusion	4-21
5. Conclusions, Recommendations, and Future Work	5-1
Appendix A. Statistical Eye Model Code - FGenEyePop.m	A-1
Appendix B. Dose Response Model - Probability to Dose - FProbToDose.m	B-1
Appendix C. Dose Response Model - Dose to Probability - FDoseToProb.m	C-1
Appendix D. Ray Trace Approximation Code - FEyeProp.m	D-1
Appendix E. BTEC Config File - Main	E-1
Appendix F. BTEC Config File - Emitter	F-1
Appendix G. BTEC Config File - Sensor	G-1
Appendix H. BTEC Config File - Layer	H-1
Appendix I. Rozema Statistical Eye Model Data	I-1
Appendix J. Quad Chart	J-1
Bibliography	BIB-1

	Page
Vita	VITA-1

List of Figures

Figure		Page
3.1.	Dose Response Curve Showing Damage Thresholds for Tissue Samples. Line A shows a deterministic response (no unknown factors) threshold at 100 mJ. Lines B, C, and D show a 1-, 2-, and n-factor variance model, respectively, each with an increasingly skewed response curve (empirical CDF) and changing mean threshold.	3-7
3.2.	Graphic showing effects of focal length on retinal spot size due to hyperopia (left) and myopia (right) compared to normal emmetropic eye (center). The change in focal length causes refractive error shifting the focal point of the light passing through to the retina.	3-10
3.3.	Rockwell ABCD model output demonstrating propagation for 6- and 3-mm beams at 1064-nm.	3-14
3.4.	Figure depicting retinal layering system used in BTEC Thermal Model simulations. Grid resolution and sizing may be varied dependent on input beam characteristics.	3-18
3.5.	Graphic showing effects of wavelength on spot size as a function of axial depth (left) and the CDF of spot size as determined by Rockwell ray trace model for a 3-mm, 514-nm laser exposure (right).	3-20
3.6.	Graphic showing comparison of BTEC Thermal Model and experimental damage threshold results, raw data as well as data corrected for species variation and transmission loss. Slightly higher experimental threshold most likely due to laser beam scattering, rhesus to human conversion factor, or effects of anesthesia on subjects.	3-21
3.7.	BTEC thermal model results for 6-mm beam at the cornea using only biological variance in focal geometry for 100-ms and 1-s exposures. Vertical lines represent Maximum Permissible Exposure (MPE) Limits for comparison.	3-22

Figure		Page
4.1.	Graphic showing comparison between a deterministic and probabilistic approach to risk modeling. The probabilistic model (left) shows a color-coded degree of risk based on a Gaussian footprint of laser energy. The deterministic approach (right) shows only a region of unsafe exposures. Calculations for elevations are excluded from this example for simplistic demonstration.	4-8
4.2.	Surface generated from BTEC simulation data for 10-millisecond exposure. Point of interest on the surface in this graphic is the 20 th -percentile (49- μ m diameter) damage threshold for a 532-nm exposure calculated at 10 milliseconds. The plot displays the interpolated surface among the blue circles representing the simulated data.	4-24
4.3.	10-, 100-, and 1000-millisecond surfaces generated from BTEC simulation data. Point of interest for this example is the 20 th -percentile damage threshold for a 532-nm corresponding to a 49- μ m diameter retinal spot size. The plot displays the interpolated surfaces among the blue circles representing the simulated data.	4-25
4.4.	PCHIP model for time dependency. Point of interest is at 250 milliseconds with a TIE dose calculated to be 770.7 microjoules.	4-26
4.5.	Probability of damage as a function of retinal dose and point result for example in this section. Plot visualizes trade-space for risk of dose between 800 and 840 microjoules.	4-27
4.6.	Plot depicting probability of damage as a function of radiant exposure for 0.3-cm pupil in daytime light conditions. Dashed line represents ANSI Z136.7-defined maximum permissible exposure (MPE) limit.	4-28
4.7.	Plot depicting probability of damage as a function of radiant exposure for 0.6-cm pupil in nighttime light conditions. Dashed line represents ANSI Z136.7-defined maximum permissible exposure (MPE) limit.	4-29

Figure		Page
4.8.	Plot depicting probability of damage as a function of radiant exposure for 0.3-cm pupil in daytime light conditions. Dashed line represents ANSI Z136.7-defined maximum permissible exposure (MPE) limit.	4-30
4.9.	Plot depicting probability of damage as a function of radiant exposure for 0.6-cm pupil in nighttime light conditions. Dashed line represents ANSI Z136.7-defined maximum permissible exposure (MPE) limit.	4-31

List of Tables

Table		Page
3.1.	Table of Mainster and DeMarco thermal properties for ocular tissues.	3-17
3.2.	Comparison of Rozema[29] data, Rozema Model, and proposed model. Proposed model output matches data and previously published results.	3-19
3.3.	Table of 0.1- and 1.0-second results. Higher probit slope values indicate smaller variance in threshold due to biological variance. MDLS (Minimum Diffraction Limited Spot Size) = 10 μm	3-20
3.4.	Results from 694-nm, 0.1-s and 1.0-s simulations using both Mainster and DeMarco thermal properties. In both cases, thermal parameter variation of approximately 10% yields a similar shift in damage threshold.	3-21
3.5.	Simulation predicted damage thresholds compared to current safe exposure limits for a 3- and 6-mm Gaussian beam. Table values are given as ratio of threshold/exposure limit. MDLS (Minimum Diffraction Limited Spot Size) = 10 μm	3-23
I.1.	Table of eye data taken from Rozema study.	I-1

List of Abbreviations

Abbreviation		Page
LTI	Laser-Tissue Interaction	1-3
TIE	Total Intraocular Energy	2-1
BTEC	Buffington-Thomas-Edwards-Clark	2-6
RPE	Retinal Pigment Epithelium	3-1
CDF	Cumulative Distribution Function	3-3
MPE	Maximum Permissible Exposure	3-4
DARPA	Defense Advanced Research Projects Agency	3-4
NOHD	Nominal Ocular Hazard Distance	4-2
Nd:YAG	Neodymium-doped Yttrium Aluminium Garnet	4-7
ABL	Airborne Laser	4-7
OCT	Optical Coherence Tomography	4-9
AFRL	Air Force Research Laboratory	4-10
MVL	Minimum Visible Lesion	4-12
PCHIP	Piecewise cubic Hermite interpolating polynomial	4-15
FDA	Food and Drug Administration	4-22

PROBABILISTIC MODEL FOR LASER DAMAGE TO THE HUMAN RETINA

1. Introduction

Since the invention of the laser in the mid-20th century, the technology has become vital to the existence of a seemingly uncountable number of commercial, academic, medical, and defense applications. The art of directing coherent light into a spatial domain with high precision allows for cutting raw materials, studying the properties of matter, non-invasive imaging of the human body, and guiding munitions to their targets. As of January 31, 2012, the United States Patent and Trademark Office Patent Application Full-Text and Image Database shows an incredible 393,012 patent applications for inventions related to laser technologies since 2001. The limitations for laser system applications are seemingly only bounded by our imagination and technological capability. Charles Townes, one of the men credited with inventing the laser, said in 1960 that it was “a solution looking for a problem” [36]. This statement still holds true today. Laser system applications are seemingly only bounded by our imagination and technological capability.

For each application, safe use of lasers with respect to injury or unsafe conditions is held in high regard. Specific safe exposure guidelines are developed for each basic family of laser emitter types grouped by beam characteristics such as exposure duration, wavelength, pulse types, and beam diameter. Tissue-specific guidelines are based on the exposed body area with a focus on the retina, cornea, and skin. For each of these exposure locations, the biological response to the light energy is classified into photothermal, photochemical, and mechanical effects, each coming from a different exposure type. Due to the sheer number of exposure types and scenarios, there is no single metric used to define a safe laser exposure.

Unsafe laser exposures may cause photothermal, photochemical, and mechanical damage to the eye and skin. Photothermal damage is the damage induced by raising the temperature of the tissue until proteins are denatured, causing loss of function. It is a primary damage mechanism observed at all laser wavelengths with exposure durations greater than a microsecond. Photochemical damage is the process of changing the chemical makeup of tissue or cells until loss of function occurs. Photochemical damage is often associated with ultraviolet wavelengths shorter than 500 nanometers. Exposure times for photochemical damage are usually tens of seconds or higher and may be observed at power levels lower than those that would induce photothermal damage. Mechanical damage effects are those created in a situation where energy is deposited in sub-microsecond pulses in a relatively small location, often creating rapid expansion of the absorbing medium until it bursts. The shockwaves from such a burst may also damage neighboring tissues.

Understanding damage mechanisms is the foundation for establishing safe exposure limits or estimating risk of injury to humans. However, this research is costly and the use of human subjects is only possible in extreme circumstances such as the removal of the eye in cases of cancerous tumors. Therefore, there is an implied limit to the amount of data that can be collected to assist in establishing safe exposure limits. Most of the biological studies focus on animal models that are carefully chosen as a replacement for human sub-systems. The rest of the data comes from modeling and simulation. The basis for choosing an animal model is how well it mimics the human eye in functionality and dimension.

These studies historically focused on determining a damage threshold for the 50th-percentile of the population as a way to state the average power that would damage a human cell, tissue, or system. This threshold is often determined using analysis methods that describe the mean value and the spread of experimental data. These two metrics are then used to determine the confidence interval about the mean value. This approach is an effective method to determine mean thresholds for

a population; however, using these measures to do any further analysis in the tails of the distribution may be problematic .

The need for a probabilistic approach to estimating damage thresholds has forced researchers to look to the decades of historical data for insights into how laser energy effects a human population. The confidence intervals about the mean threshold were taken from the spread of the data under the assumption that damage thresholds follow a log-normal distribution. The mean value is reported along with a slope value derived from the location of the data influenced by the amount of variance in threshold results. This variance comes from experimental error, limits on precision and accuracy, and biological variance between samples. Reporting the spread of data with one parameter effectively marginalizes each source of variance and confounds it to one statistic.

Damage threshold research is intended to create safe exposure limits influenced primarily by the biological response of the experiment. Therefore, the influences of biological variance must be considered separately and held isolated from the other factors. This research effort focuses on the development of a model to isolate the biological influence in a probabilistic manner by developing a statistical model eye. Photothermal damage thresholds are examined in the time domain of 10 to 1000 milliseconds for visible and near infrared wavelengths in the range of 514 to 1064 nanometers. The statistical model eye generates a population eyes using a covariance structure derived from human data for input to a propagation model. The propagation model determines the retinal spot size using a ray trace algorithm. This in turn is used as an input to a laser-tissue interaction (LTI) model to estimate the damage threshold for each empirically-determined percentile. The final distribution of damage thresholds is used to create a probabilistic dose-response model for the experimental region.

The need for probabilistic dose-response models stems from the need to analyze the risk of using lasers at estimated unsafe power levels. Better probabilistic models

can serve to improve safe exposure limits. Furthermore, once safe exposure limits have been re-examined and potentially revised, the dose-response model can be used to assess risk with more accuracy. Laser applications in defense, medicine, and research will benefit from the probabilistic approach to modeling laser damage thresholds described in this research.

The format of this document is two separate papers. The first is the development of the statistical eye model based on human covariance data. The paper examines trends in wavelength and time dependencies of damage thresholds. The research and findings were presented at the annual SPIE Photonics West Conference in San Francisco, January 24, 2012. The second paper is the application of the statistical eye model in the creation of the dose-response model. The model can be used to establish the design space in the development of future laser systems or in the development of doctrine, tactics, techniques, and protocols for new or established systems. Additionally, it provides the foundation for a true population-based risk analysis tool for safety standards development.

2. Background

This research effort stems from the need to understand and quantify the biological influence on decades of laser damage threshold data. Historically, laser damage threshold experiments report the threshold results of the binary response, of either damage or no damage, for a given stimulus in terms of laser power using probit analysis metrics. D. J. Finney developed this method and published a book in 1947 [9] describing how to estimate the probability of a positive response as a function of a continuous domain of the stimulus. The most frequently reported statistic from probit analysis is the ED_{50} value, the level of stimulus associated with a 50% probability of a response. In laser damage threshold experiments, this is the amount of power, or dose, of laser energy associated with a damage response event in 50% of the target samples.

Dose may be calculated with respect to total energy measured in joules (J) or watts (W) ($1\text{ watt} = 1\frac{\text{joule}}{\text{second}}$), or by energy in terms of density defined by the size of the beam. Power density may be measured in radiant exposure, $\frac{J}{\text{cm}^2}$, or by irradiance, $\frac{W}{\text{cm}^2}$. In the experimental database used in this study and maintained by the Air Force Research Laboratory's Tri-Service Research Lab in San Antonio, Texas, more than 1,200 damage thresholds are reported as total intraocular energy (TIE). This calculation accounts for pupil size and the is measured strictly in joules or microjoules. For the purposes of this study, all reported thresholds are reported in terms of TIE except where specifically noted.

Since ED_{50} is a mean value of the doses that caused damage in a sample population, it is implied that doses lower and higher than ED_{50} exist as damage thresholds. The probit slope describes the spread of the threshold data. Sliney et al. [33] calculate this slope using the ratio of ED_{84} to the ED_{50} , where ED_{84} is the level of stimulus associated with an 84% probability of a response. The 84th percentile comes from statistics where the cumulative distribution function of an assumed nor-

mal distribution is equal to 0.84 at a distance of one standard deviation higher than the mean. Some experiments cite the ED_{16} to reflect the same information. Additionally, probit analysis in laser damage threshold research assumes a log-normal distribution of damage. Therefore, many of the calculations require a logarithmic transformation.

The techniques involved in probit analysis were initially developed for toxicology studies where each test could logically be considered separate and independent to estimate lethal doses of pesticides. Sliney describes the adaptation of probit analysis to laser damage threshold studies to be problematic as the underlying assumptions cannot be made. In damage threshold studies, cost and resources are often limiting factors. Therefore, many experiments involve the same subject in multiple exposure locations. Rather than characterizing this sampling technique as multiple independent exposures, it is a replicated sampling of the same subject multiple times which will work to influence the standard deviation and variance of the data.

This and other influences on the variance of the data cause issues to arise with adopting the probit techniques to laser damage threshold studies in order to examine probabilistic responses at doses other than the ED_{50} threshold. Musch [23] and Wolbarsht [41] support this and also claim that ED_{50} values are also influenced simply due to the definition of damage. Damage is not a precise endpoint since characterization of damage may vary between experiment, observation, or equipment conditions. For example, one experiment may use special high-resolution imaging techniques to determine if a lesion is present with a minimum radius. Other experiments may use the same exposure and laser beam parameters but define damage by a recognizable lesion on the retina through an aided viewing device such as a fundus camera. Both will report damage threshold for a given exposure and laser setting but the thresholds may vary greatly because the measure and method of response was different. These differences are understood and estimates are used in normalizing thresholds dependent on how the ED_{50} was determined; however, these are only estimates so

they do not entirely eliminate the influence of this variance on the reported thresholds. Exposure location on the retina is another factor that influences damage. The macula is where the light focuses to provide central vision. It is much more sensitive and has a lower damage threshold than the areas outside of the macula, known as the paramacular region. Researchers also normalize for this shift in threshold but the conversion factor is only an estimate, therefore inducing another source of variance.

The theoretical probit slopes of 1.05 to 1.15 calculated by Sliney et al. suggest that an ED_{50} threshold given in logarithm base 10 units equal to some value X_{50} will have an ED_{84} between $10^{1.05X_{50}}$ and $10^{1.15X_{50}}$, or between 11.2 and 14.1 times higher than the reported ED_{50} . In some cases, it was reported that experimentally collected data often exhibited probit slopes of 1.5 to 1.7. These slopes represent ED_{84} powers between 31 and 50 times the ED_{50} values. These results indicate an extremely large variability in threshold results that cannot be explained by theory. This increased variability may influence the reported ED_{50} thresholds but its effects are more detrimental to the tails of the probability distribution. Safe exposure limits are based on the spread of data almost as much as the threshold itself in order to ensure they exist below the lowest doses where damage may occur. Previously established exposure limits and dose-response models are based on existing research but may be improved through a better understanding of these effects and quantification of the underlying distribution's influences. Improvements may include changes to the linearity of exposure limits with respect to wavelength to raise exposure limits closer to the predicted laser powers where damage may be possible, eliminating unnecessarily large safety buffers.

Schulmeister et al.[31] agrees with Sliney's findings and provides an in-depth review of many supporting factors. This work includes a detailed explanation of how other experimentally controlled factors can not be known with exact precision or accuracy, introducing yet another source of variance. Inter-subject variance is also mentioned as a source of overall uncertainty in establishing damage thresholds. For

retinal studies, different ocular structure characteristics can influence how the laser light propagates through the eye and, in turn, the biological response to the photons at the retina. These characteristics include geometrical, thermal, transmission, and other physical properties of the eye.

Physical differences between the focal geometries and ocular structures eyes create a variability in how the light arrives at the retina. Out of tolerance deformities create refractive errors, increasing the laser spot size on the retinal plane and affecting the power density calculated at the retina. Although some corrections are made for refractive error in experiments, small deviations may still exist. This variance in power density influences the reported damage threshold because the amount of energy at the exposed area of the retina is different. For larger refractive errors, the spot size on the retina increases. For example, two identical laser beams enter two different eyes with a power of 50 microjoules. The first eye has a refractive error of zero while the second eye has one diopter of refractive error. According to Schulmeister, the first eye with near perfect vision would place the laser beam into a tight spot on the retina with a diameter of 10 micrometers. The second eye with the one diopter error would negatively influence propagation and yield a 127 micrometer spot at the retina. The resulting power density is 161 times lower for the eye with the refractive error. This is indicative of the extremely high impact biological variability has on damage threshold variance.

It is important to note that the one diopter of error is the average refractive error for the human young adult population [19, 8]. Refractive error has many causes including poorly shaped or sized eyeballs, corneas, and lenses. The eye works to accommodate for this error by adjusting the shape of the crystalline lens using small muscle formations within the eye. The amount of accommodation is approximately one diopter in refractive power [24]. Therefore, the human eye, on average, can adjust and compensate for the average refractive error.

Statistical distributions of refractive error show an approximately normal behavior with a mean value of approximately -1 and standard deviations between 1 and 2 diopters [19, 8]. This information could be used to develop an approximation of spot size based on the distribution of refractive error but it may lead to problems. Chromatic aberrations, a term used to describe the wavelength dependence of light propagation in the eye, must be accounted for in any model developed to simulate laser propagation [27]. Therefore, a more geometry and wavelength specific model for propagation is required.

Ray tracing models based on complex Gaussian beam propagation may be used to predict spot size on the retina for a given set of input beam parameters. The method uses spatial dimensions for the ocular system components and their indices of refraction to determine the behavior of laser propagation. The method developed by Rockwell et al.[27] is shown to predict spot size and account for chromatic aberration. The study was validated against fiber probe and laser induced breakdown techniques. The input needed for the Rockwell model included specific eye measurements such as lens and cornea radii of curvature, vitreous and anterior chamber depths, and lens and cornea thickness.

The summary statistics for mean and standard deviation data of ocular system components is readily available in literature. Studies such as a bridge study conducted at the Air Force Research Laboratory to investigate alternative animal models for research [26] included not only these parameters for humans, but for two other animal species as well. These studies report the specific eye measurements needed for the ray tracing model previously mentioned. However, in order to create a complete and sound statistical model, one must have all the information available about each individual component's means and standard deviations, as well as the covariance structure among the sample data. The covariance structure describes the relationships of one component with the others. Therefore, a random draw from a statistical distribution of lens thickness will intelligently influence the random draw

from the statistical distribution of the lens' anterior and posterior radii of curvature. This type of relationship exists in the covariance structure.

In 2011, Rozema et al.[29] published the results of a model eye based on the complete covariance structure of 127 human eyes. The resulting model matched the true human measurements with excellent agreement and reproduced a similar covariance structure. The Rozema data and method is selected as the foundation for the development of the statistical eye model in this research. The model is slightly modified to improve the influence of missing data through some mathematical methods originating in financial applications.

The statistical eye model is sampled 50,000 times to provide input to the ray trace model. The results for input beam wavelength and beam diameter generate empirical cumulative distribution functions for retinal spot size. The model output from this research for a 514-nanometer beam with a 3-millimeter pupil is a 124 micrometer spot size diameter. This showed agreement with Schulmeister's reported 127 micrometer spot size diameter. Both of these are based on an average refractive error of -1 diopter.

Once the laser energy has propagated through the eye, it reaches the retinal surface. Here it must be absorbed, reflected, or transmitted. The absorption of photons from the laser beam induces a temperature rise. The temperature rise is one of the critical components in laser-tissue interaction (LTI) simulations. The time-dependent photon absorption as distributed across a discrete grid is known as the source term used in solving the heat equation. The solution of the heat equation in spatial and temporal domains defines a time-temperature profile for any given point in the simulation space. A rate process model then integrates temperature over time using normalized parameters of the Arrhenius Integral to estimate whether or not damage has occurred.

LTI simulations such as BTEC Thermal Solver [15] are deterministic in nature with respect to estimating thermal rise and damage. This study utilized the BTEC

code because of availability and ease of configuration and its continued validation against experimental results [4]. Each unique BTEC input results in a unique output. In order to use the model in a probabilistic fashion, the input parameters are sampled from a probability distribution and results linked to the probability of observing the input configuration. If an input is selected by choosing the 50th-percentile of data, the resulting damage threshold prediction is considered the ED_{50} . This methodology is the foundation of using a probabilistic model to predict the laser beam spot size on the retina. Other parameters such as thermal properties and physical dimensions are also configurable to meet the user's needs.

The BTEC Thermal Model's deterministic nature enables the simulation to precisely and accurately define any input parameters. An input beam diameter and power are used in the solution as exact parameters. In the real experimental world, these factors have some inherent error due to measurement capability. By fixing parameters such as these, only those parameters intended to vary will affect the outcome. This enables one to study the effects of one or more input variables in order to examine individual effects on the solution space.

One limitation of BTEC is the inability to model non-uniform tissue layers. Each layer used in the model is assumed to be a spatially averaged mass with a resolution on the order of micrometers. In retinal simulations, for example, cells on the retinal layer are significantly different than in the neighboring layers but cannot be distinguished within the uniform layer. Since most cases of this research effort will examine relatively large areas of the retinal, averaging is not predicted to have substantial impact on the results.

The following chapters document stand-alone research efforts examining how to use the information presented here to adapt existing models to build probabilistic models for laser damage to the human retina. Chapter 3 was presented to the International Society for Optics and Photonics at the 2012 Photonics West Conference. It generated interest from international colleges, representatives from the Depart-

ment of Defense, and the United States Food and Drug Administration. Each of these organizations has a vested interest in damage threshold research and it is my wish that this thesis provides a strong foundation for developing a new approach to research and system development methodologies.

*3. An Analysis of the Influences of Biological Variance,
Measurement Error, and Uncertainty on Retinal Photothermal
Damage Threshold Studies*

This chapter is the conference paper presented at SPIE Photonics West, BiOS, at San Francisco, California, on January 24, 2012. It is currently in review for publication in the proceedings as paper 8221-40 [42]. Publication date is estimated to be March 2012.

3.1 Abstract

Safe exposure limits for directed energy sources are derived from a compilation of known injury thresholds taken primarily from animal models and simulation data. The summary statistics for these experiments are given as exposure levels representing a 50% probability of injury, or ED_{50} , and associated variance. We examine biological variance in focal geometries and thermal properties and the influence each has in single-pulse ED_{50} threshold studies for 514-, 694-, and 1064-nanometer laser exposures in the thermal damage time domain. Damage threshold is defined to be the amount of energy required for a retinal burn on at least one retinal pigment epithelium (RPE) cell measuring approximately 10 microns in diameter. Better understanding of experimental variance will allow for more accurate safety buffers for exposure limits and improve directed energy research methodology.

3.2 Introduction

Developing directed energy systems requires an understanding of how each type of energy source affects an exposed material, either living or non-living. Directed energy effects on living tissues of persons or animals are often complex due to the non-uniformities between regions of the body and within the populations as a whole. Determining the degree of influence of experimental error, uncertainty, and biological

variance requires a great deal of experimental research as well as modeling and simulation of these systems.

Laser-tissue interaction (LTI) modeling and simulation helps to supplement costly experiments on living tissues and employs the use of deterministic, first-principles, multiphysics numerical simulations to predict how tissues exposed to directed energy respond. In the case of retinal damage threshold research, LTI models supplement studies using enucleated eyes or animal models in order to provide a less costly means of estimating the effects of a laser exposure on these tissues. The model estimates interaction effects such as energy absorption, scattering, and transmission through a medium and uses this as an input to a thermal damage model.

Biological variance, error, uncertainty, and laser exposure parameters that include wavelength and exposure duration are critically influential factors in LTI. Rather than a simple point estimate representing a damage threshold, a range of exposure levels are required to express what level of energy, or dose, will produce a given response such as a burn, lesion, or hemorrhage. Therefore, any attempt to establish safe exposure limits should account for these factors. For years, researchers examined families of exposure types classified into damage mechanisms, time dependency, wavelength, beam characteristics, and others, to predict each family's distribution of damage. Increased sample size, improved equipment precision, and accurate experimental design improve the quality of these results; however, biological differences within a population will always remain a significant source of threshold variance. This research examines how variance in an eye's focal geometries and thermal parameters impact damage thresholds of the retina.

3.3 Background

Statistical variance in threshold studies plays a significant role in directed energy biological effects, or *bioeffects* research. Generally, inter- and intra-subject variations guarantee a range of damage threshold values rather than a single exper-

imental endpoint. These ranges are reported using descriptive statistics, typically a mean and a measure of variance that describes the spread of the data. Determining the degree of influence for each source of variance in damage threshold studies is a crucial factor in determining a population's damage threshold characteristics. Understanding the root causes of threshold variance is important in the development of safe exposure limits because many aspects used in their determination is based on a probabilistic approach. Optical, thermal, geometric, and physical properties of tissues are sources of biological variance considered in this research.

Most damage threshold studies dating back to the mid-20th century use probit analysis[9] to quantify the sample variance, experimental uncertainty, and measurement error, in damage threshold studies as a combined variance metric. Probit was developed “to help biologists whose acquaintance with statistical method was slight and who were naturally hesitant to undertake calculations that seemed difficult (and) laborious”. One of its earliest applications was in toxicology lethality studies to quantify a binary response, either lethal or non-lethal, within a population such as insects or rats. In directed energy research, probit analysis assumes a log-normal distribution of a dose level required to elicit a binary response, damage or no damage, and translates the data into an empirical cumulative distribution function (CDF). The most important results of probit analysis are the empirical 50th-percentile, ED_{50} , and the probit slope, a variance measure determined by the relationship between the ED_{50} value and either the 16th- or 84th-percentiles. The central limit theorem guarantees that increasing the sample population through experiments with similar exposure parameters will ultimately determine the true population mean damage threshold but any sources of inherent variance prohibit convergence to a single damage threshold for the entire population.

Uncertainty, error, and variance come from many sources. Researchers may occasionally make observation errors when attempting to classify a result as a binary damage response when examining a 10- μm diameter lesion on the retina through a

fundus camera. Power density is recorded by a device with imperfect precision. Biological variance between subjects may also create a condition where the same laser exposure to one subject or location creates an observable lesion but has no response with another. As damage threshold research matures with time, methodology and quality of results improves. The observers will better view the same microscopic lesion that was previously unrecognized through the use of better equipment. Future measurement errors will be reduced using more advanced equipment. However, biological variance will still remain a factor and must be quantified.

Developing safe exposure limits for lasers is one of many real world applications of damage threshold studies. The ANSI Z136 [1] series provides maximum permissible exposure (MPE) limits for lasers for industry, education, and military application and research. The military shows its appreciation for directed energy systems by its vast proliferation of laser target designators, range finding equipment, non-lethal laser glare applications, and munitions guidance systems as well as the relatively large annual budget allocation to future technologies programs under the direction of the Defense Advanced Research Projects Agency (DARPA)[7]. Higher powered laser systems offer a potentially new class of weapons enabling line-of-sight at the speed-of-light engagements with a potentially lower degree of collateral effects compared to traditional kinetic munitions. However, development of such systems and the quantification of their collateral effects relies on the understanding of biological responses.

In order to determine a safe exposure limit, it is vital to understand the probability distribution of damage thresholds, especially in the lower tails of the empirical CDF. Current MPE limits are typically defined to be a fraction of the experimentally determined ED_{50} values. This fractional safety factor takes into account the experimental uncertainty, error, and variance. However, due to the spread of the experimental data, there may exist some cases where a fixed fraction of ED_{50} for a given exposure may lie uncomfortably close to the empirical CDF's lower tails due

to the influence of uncertainty, error, or variance. In other cases, the spread of data may be much more compact and the MPE limit can be unnecessarily restrictive. Modern research[31, 23] is beginning to stray from this classical approach and seek alternative methods of modeling variance in lieu of a fixed fractional safety margin. It is imperative that statistical methods used in safety research are “difficult and laborious” to carefully place bounds on the degree of influence for each independent source of variance in order to better quantify risk for safe exposure limits research. Probabilistic risk modeling is an associated application that has already begun utilizing alternative approaches[2, 31].

Each source of variance must be quantified in order to create a useful probabilistic model but each source may require multiple studies to accomplish this task. Retinal ED_{50} studies are often cost prohibitive and may only address one of many unknowns at a time. In 1999, Zuclich et al.[43] reported on the relationship between spot size and damage threshold. Kennedy and Zuclich [20] reported in 2004 on the variation in retinal image size but varied beam profile characteristics. In 2007, Lund et al.[21] examined a similar relationship but varied wavelength. Follow-on studies such as these bolster the body of bioeffects research because they decrease the uncertainty in some areas, increase the overall sample size, and provide more experimental results. Furthermore, they introduce and help to quantify new sources of variance such as the influence of subject-to-subject variability with the new samples taken from a population. By performing these studies over time, researchers can reduce the influence of threshold variance from uncertainties or errors and identify those biological influences that may explain a true distribution of damage thresholds for a given population.

As an illustrative example, consider a single RPE cell in a controlled water bath, or *in vitro* latin for *in glass*, that is exposed to a laser such that power density, wavelength, and exposure duration are known with infinite precision. The single cell thermal damage threshold is the exposure level required to increase the temperature

of the cell high enough to cause an observable, thermally-induced protein denaturation. The empirical CDF relating the probability of damage to laser power based only on this single exposure is a step function having a value of zero for powers lower than the threshold and a one for powers greater than or equal to the threshold.

Repeating the experiment described above using RPE cells drawn from a sample population will result in a range of powers and a binary response of either “damage” or “no damage” for each. Assuming each of the other experimental parameters are constant, the population variance creates a measured spread of the data. This set of data having a mean and measure of variance is used to create a 50% probability of damage estimate and associated confidence interval.

In the case of *in vivo*, or *within the living*, experiments, optical, physical, thermal, and geometric properties impact laser energy propagating through the eye. Variation in the geometry of the eye greatly impacts this propagation and, ultimately, the laser spot size on the retina. This in turn affects the reported power density at the retinal plane. Thermal properties of the retina such as conductivity and specific heat also vary[6]. As these additional 1, 2, ..., n additional sources of variance are introduced, what was originally a random variable with a mean and variance becomes a random variable from a probability distribution determined by the convolution of n random factors and their individual distributions. Such a distribution may cause the damage threshold to vary greatly so it is important to quantify each of the most dominant factors that influence threshold. Figure 3.1 illustrates the relationship between a notional 1, 2, 3, and n -factor variance model.

Human experimentation is the ideal approach for determining human safe exposure limits but it has only been conducted in a relatively few cases such as those where the enucleation of the eye is required [37]. Since threshold studies require many exposures for each combination of wavelength, exposure time, spot size, pulse train and other determining factors, a means to study an optical system similar to the human eye is required. The primary method of finding damage thresholds for the

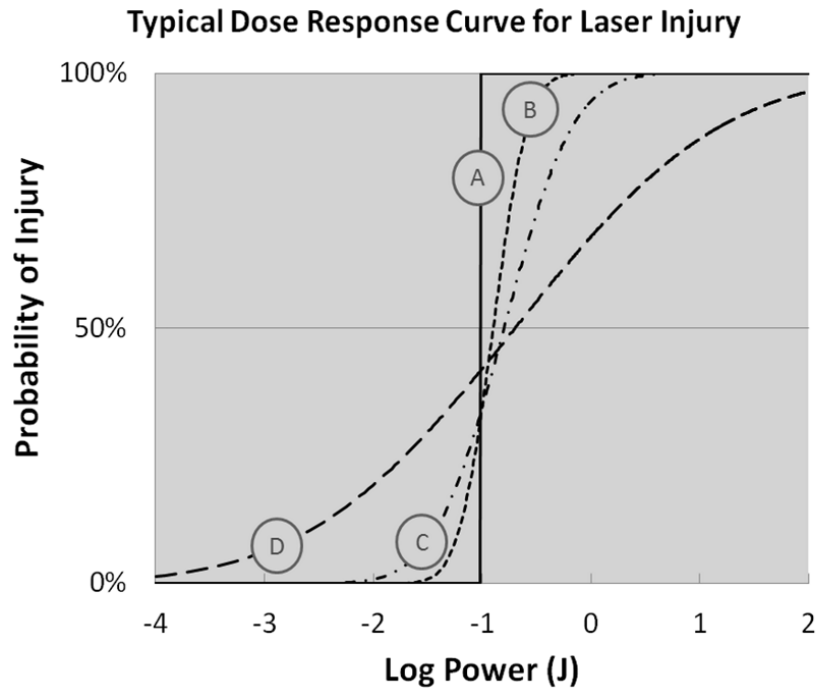


Figure 3.1 Dose Response Curve Showing Damage Thresholds for Tissue Samples. Line A shows a deterministic response (no unknown factors) threshold at 100 mJ. Lines B, C, and D show a 1-, 2-, and n-factor variance model, respectively, each with an increasingly skewed response curve (empirical CDF) and changing mean threshold.

living eye is the use of an animal model under the strict supervision of an AAALAC accredited laboratory. The Indian-origin rhesus monkey (*Macaca mulatta*) has been the primary animal model used for testing retina thresholds for nearly 50 years. However, it possesses a slightly smaller eye than a human and the focal geometries are somewhat different, yielding a decrease in the mean threshold ED_{50} . With respect to animal models such as the rhesus monkey, differences between these surrogates and humans can create a shift in the mean threshold. Furthermore, rhesus eyes are much smaller and vary much less with respect to size than the human eye [26] and suggest not only a shift in the mean, but a more compact data spread and empirical CDF. The consequences of such a relationship suggest that assumptions used when predicting human thresholds based solely on the rhesus model must be carefully evaluated. Although Rongjia et al.[28] have published some results stating that the

mean damage threshold values for rhesus-to-human are approximately 1:1.765, this can only be applied to the ED_{50} because other values such as the 10% threshold, or ED_{10} , are not a simple linear transformation given the more compact CDF.

Although animal subjects are much more accessible than human subjects, they are very costly. In an effort to reduce costs through innovation, scientists often choose to utilize computer modeling and simulation in lieu of experiments. Computer simulations such as the Buffington-Thomas-Edwards-Clark Thermal Model (BTEC) [15] or COMSOL, a commercially available multiphysics tool, are used in place of these physical experiments. These simulations help to fill in the gaps where experimental data is not available. Simulations also assist in planning real world experiments by determining which new data may be valuable, helping to save incredible amounts of time and money. BTEC is frequently validated by experimental work and is used to generate derivative models[4]. Built upon first principles physics simulations, BTEC uses a variety of propagation methods to distribute directed energy throughout a system, typically the skin or the eye, where its absorption, reflection, scatter, or transmission is recorded over a specified time period. The profile of energy within a given one- or two-dimensional system is known as the source term for the heat equation. This is used to directly determine damage based on the induced temperature profile over time using an Arrhenius rate process model. This research effort will employ the BTEC thermal model due its availability through cooperation with the Air Force Research Laboratory.

Even with the best tools available, modeling the eye is a complex endeavor. The nature of the eye is to accommodate vision and to focus light onto the retina in a small area known as the macula, where the density of photoreceptors is highest and therefore enables the most precise visual response. Proper calibration of the visual system ensures that light reaches these photoreceptors at the right angle and focal point. Small defects may exist within the vision system but the human eye can actively adapt to allow for small deviations to be within visual tolerance. A well-

formed, or emmetropic, young adult eye averages 23.5 mm [26, 29] allowing light reflected from an object to focus onto the retina. Conditions of myopia (nearsightedness) and hyperopia (farsightedness), collectively known as ametropia, adversely affect the focus of the retinal image. These conditions are common with varying degrees and are caused by imperfections in the focal geometry of the eye. As an infant, the eye is disproportionately small causing light rays to be directed behind the retinal plane by the cornea and lens causing axial hyperopia. As the body grows into adulthood, usually the eye and its components grow relatively more proportionate, pushing the retinal plane back to meet the natural focus. Eye growth begins to slow as adulthood is reached, but it does not cease. Later in life, the retinal plane will extend beyond the focal point of light causing axial myopia. This may explain infants cannot see something that is too close to their face and may also explain why older humans must hold text closer to their eyes to see it. Although natural aging and growth processes can create conditions of hyperopia and myopia, a significant sub-population exhibits these conditions throughout life due to out of tolerance focal geometries of the cornea and anterior portions of the vision system. In contrast to axial ametropia, refractive ametropia is a condition where the poorly shaped cornea creates a focal point in front of or behind the natural retina plane.

Another significant refractive error is astigmatism. This refractive error is caused by a poorly-shaped cornea or globe, creating a change in the focal point on the retina. Astigmatism is a common occurrence and is often coupled with myopia and hyperopia further impacting the focus on the retina.

The degree to which the visual system is within tolerance, enabling uncorrected sight, is often described by refractive error. Eyeglasses and contact lenses are able to correct for refractive errors by reforming the light entering into the cornea, correcting the focal position on the retina. In recent years, surgery on the cornea itself has been a means to provide vision correction to those suffering varying degrees of ametropia.

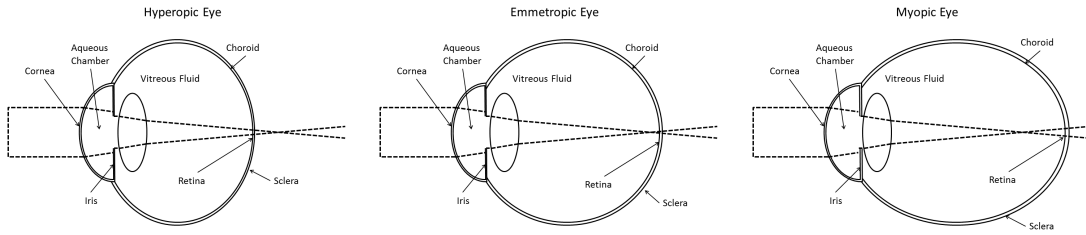


Figure 3.2 Graphic showing effects of focal length on retinal spot size due to hyperopia (left) and myopia (right) compared to normal emmetropic eye (center). The change in focal length causes refractive error shifting the focal point of the light passing through to the retina.

Another source of biological variance of the eye is the quality and characteristics of the crystalline lens. The small variances in the shape and size can greatly influence the spot size on the retina while the transmission problems of the lens such as cataracts can create loss in the total amount of light reaching the retina. Furthermore, the lens is an adaptive part of the optical system making it complicated to model. The optical system forces the lens to change shape as vision must accommodate to view objects not easily seen with a relaxed lens. Additionally, the non-uniform refractive index of the lens effects light propagation. Lenses are often modeled as having a uniform index that is an overall refractive power but some modeling research utilizes a gradient index, continuously changing from the anterior to the posterior surfaces of the lens. This research effort varies the size and shape of a relaxed lens and assumes a uniform refractive index using the average power of the lens. Accommodation and gradient indices as well as lens defects may also prove to be substantial influences but are beyond the scope of this paper.

Refractive error corrections for myopia and hyperopia are measured in diopters, a measurement unit of the inverse focal length ($1/m$) with a positive or negative characteristic. The human eye can actively adjust to small refractive errors in its depth-of-focus within ± 1 diopters [24]. Beyond this range, corrections are required to improve vision quality. Someone with a case of nearsightedness will require a negative refractive power correction using a concave lens in order to bring the focal

point of light properly and within tolerance into the retinal plane. On the other hand, someone with hyperopia will require a corrective convex lens with a positive refractive power.

The effects of refractive errors on retinal spot size have also been examined[31]. However, determining the source of refractive error in order to better predict spot size can be problematic. In order to examine how these conditions impact damage thresholds due to the spot size variations they induce, probability distributions of these disorders must be characterized for a given population. Previous studies have characterized the distribution of refractive errors[19, 8] and it may be possible to generalize the distribution of spot size given the effect and distributions of refractive error. However, a better alternative to this would be to model the eye using data collected from a sample population and then use the descriptive statistics and covariance data to generate a random sample of eyes with correlating geometries and propagation related characteristics.

Rockwell et al.[27] have developed a model that accepts specific geometries and other optical characteristics and uses them to determine the wavelength dependency of spot size based on chromatic aberration, a term used to describe the shifting of the focus of visible and invisible light along the axis of the eye. In this research, optical and physical parameters from an eye are used in a ray matrix propagator to determine the spot size on the retina given an input corneal spot size and wavelength. Using this method coupled with artificial eye data for a sample population, a distribution of spot size on the retina may be achieved. This approach is better than assuming a distribution of spot size based solely on refractive error because of the numerous sources and difficulty in quantifying their impacts. Rozema et al.[29] collected measurements from a population of human eyes and reported on the correlations between the optical components that provide the input variates for such a model. Their efforts were focused on improving statistical eye models in general but

only required minimal pre-processing to create a population distribution for input into the Rockwell model.

It is our hypothesis that the distribution of refractive errors across a given population is the foundation for the most influential factor of biological variance impacting light propagating and focusing on the retinal plane due to the impact on the size of the spot in which the laser energy is absorbed. Thermal properties are also examined as an additional source of variance.

3.4 Method

The primary focus of this research is to quantify the influence of focal geometry and thermal property variance in LTI damage threshold studies. Numerical simulations are performed using a validated artificial population of eyes in order to determine the empirical CDF slopes and contrast each with the safety factor built into the safe exposure limits. Other sources of variance such as power density measurement accuracy and precision should be considered a linear influence. For example, if the measured result is off by 5%, the resulting threshold values are shifted linearly in the direction of error.

Focal geometries of the eye are extremely influential to ED_{50} thresholds due to the relationship of spot size diameter to area. For a one-percent change in spot size diameter, there exists a two-percent change in area for which to deposit a constant amount of laser energy. A 10% diameter increase will yield a 21% difference in area, and so forth. The focusing of light onto the retina is extremely sensitive to the shapes, thicknesses, and relative positions of the optical system components. Two methods were evaluated to estimate spot sizes and distributions among a population.

The first method examines the findings of Schulmeister et al [31] with regards to spot size's relationship to refractive error. This method involves researching probability distributions of refractive error across populations. By using these population distributions, retinal spot sizes are determined by an approximation relating size to

refractive error for predetermined population percentiles. These spot sizes could then be used as inputs for simulation to determine the k^{th} -percentile damage threshold for a given laser exposure. However, refractive errors are caused by many factors such as astigmatic conditions, axial length variations, and corneal surface imperfections, that may exist independently of each other within the same eye. Therefore, spot sizes could not easily be determined using a one-to-one refractive error-to-spot size assumption so an alternative approach is necessary.

The second approach utilizes propagating a given laser beam of a specific wavelength and beam characteristics through the optical system onto the retina. The propagation method used by Rockwell et al.[27] is implemented using an input vector drawn from a covarying probability distribution of parameters taken from human eyes. This method accounts for chromatic aberrations and determines spot size on the retina as a function of wavelength. The ray matrix propagator used in this method accepts a Gaussian beam input and calculates the output beam based on the refractive indices, radii of curvature, and distance of propagation. The Rockwell model was provided courtesy of the Air Force Research Laboratory's Human Effectiveness Directorate, Directed Energy Division, Optical Radiation Branch, Fort Sam Houston, Texas. The original model was built using MathCAD and ported to MATLAB for ease of integration with the other components of this modeling effort.

The Rockwell model uses the complex Gaussian beam propagation parameter to calculate the spot sizes in and out of each surface from the cornea to the retina. This relationship is defined by:

$$\frac{1}{q_i} = \frac{1}{R(z)} + i \frac{\lambda}{\pi w^2(z)} \quad (3.1)$$

$$q_f = \frac{Aq_i + B}{Cq_i + D} \quad (3.2)$$

where z is the propagation distance along the axis, q_i and q_f are the complex beam parameters in and out of a surface, respectively, and $R(z), w(z)$ are the radius of curvature and spot size (radius), respectively. A, B, C , and D come from the ray matrix as

$$\begin{bmatrix} A & B \\ C & D \end{bmatrix} = \begin{bmatrix} 1 & d \\ 0 & 1 \end{bmatrix} \quad (3.3)$$

for propagation through a medium and

$$\begin{bmatrix} A & B \\ C & D \end{bmatrix} = \begin{bmatrix} 1 & 0 \\ \frac{n - n'}{Rn'} & \frac{n}{n'} \end{bmatrix} \quad (3.4)$$

for propagation at a medium change. The values n and n' are the prior and post medium refractive indices and R is the radius of curvature of the refracting surface. Propagation for 3- and 6-millimeter Gaussian beams shown in Figure 3.3.

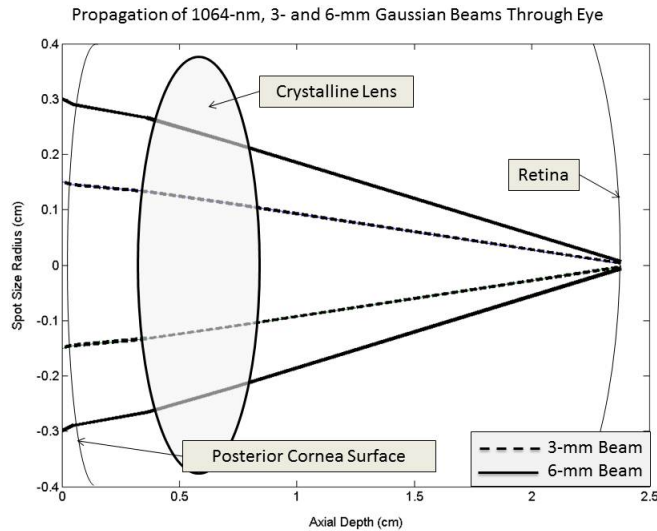


Figure 3.3 Rockwell ABCD model output demonstrating propagation for 6- and 3-mm beams at 1064-nm.

These matrices require propagation distance, radii of curvature, and refractive indices for each component within the optical system. Rockwell published wavelength dependencies for the refractive index values used here. However, determining the distribution for the other inputs required the recreation of a population using a vector of means and a correlation or covariance matrix. These are required in order to determine how a factor such as eye axial length is related to other factors such as lens thickness, as these and others cannot be assumed to be independent of each other.

The Rockwell ray trace method is used in conjunction with the eye data Rozema et al.[29] collected from 127 subjects. Raw data provided by Dr. Rozema helped to ensure each measured parameter comes from a normal or near-normal probability distribution and is reported with covariance relationships. The original covariance matrix is modified to account for missing data and for the addition of other parameters required by the Rockwell model not originally reported by Rozema. The missing values create a non-positive definite matrix, a problem for the MATLAB model developed to create multivariate random input vectors with covariance for the Rockwell model. Therefore, the covariance matrix is adjusted slightly. Rozema suggests augmenting the matrix by replacing the zero values from missing data entries with an arbitrarily small value, $\epsilon = 10^{-5}$. While these values are small, relative scaling may still lead to problems.

The process to create a best approximation of indefinite matrices due to missing data is described by Wang and Liu[38]. By adding a numerically small diagonal matrix, E to the covariance matrix, Σ , a new positive-definite or semi-definite matrix, $\tilde{\Sigma}$, is formed. The adjustment is known to introduce bias so it is important to minimize the values on the diagonal of the matrix, E . Higham[14] describes this process for dealing with non-positive definite matrices in financial applications. This approach should be a slightly more optimized approach than the method of replacing all zero values of the original matrix with $\epsilon = 10^{-5}$.

The correlation matrix, R , calculated from the original covariance matrix, Σ , is chosen in this effort due to scaling issues and correlation information relating to other parameters. Following the process described by Higham to optimize the matrix E as to minimize the introduction of bias, spectral decomposition is performed on the non-positive definite correlation matrix, $R = Q\Lambda Q^T$, where Q is an orthogonal matrix and Λ is a diagonal matrix composed of the elements λ_{ii} , representative of the eigenvalues of the matrix, R . Then, let D be a diagonal matrix with elements $d_{ii} = \max(0, \lambda_{ii})$. This will replace all negative elements of Λ with 0. Next, create the modified correlation matrix $\tilde{R} = QDQ^T$. \tilde{R} , is the closest semi-positive approximation of the original correlation matrix, R , with respect to the Frobenius norm, a measure of matrix influence. The matrix, E , can be determined by $E = \tilde{R} - R$. This optimized matrix is now a semi-positive definite or positive definite matrix acceptable for this model.

Another source of biological variance considered in this study is the variation in thermal properties of the retina and the influence on damage thresholds. Full population distributions of these are not yet readily available in literature so the variation here will be modeled using two sets of thermal properties based on the findings of Mainster and DeMarco[6] to determine the influence on damage threshold. The Mainster properties assume the eye possesses the same thermal conductivity and specific heat as water. DeMarco proposed these properties do not accurately represent the eye and chose to use the parameters of gray matter based on similarities in the high concentration of neural cell bodies. These two slightly opposing views provide approximately a 10% fixed variation for this study.

The BTEC thermal model is used to model exposures to the retina using exposure durations of 0.1 and 1.0 second at 514-, 694-, and 1064-nm, and compared to similar experimental data for validation. Although the aversion response to a bright visible wavelength laser takes generally 0.25 seconds, a whole second is modeled to capture time dependency effects. Furthermore, the 1064-nm near-infrared exposure

Table 3.1 Table of Mainster and DeMarco thermal properties for ocular tissues.

Layer Parameters		
Vitreous	Mainster	DeMarco
Thermal Conductivity (J/(s * cm * deg C))	0.00628	0.00594
Specific Heat (J/(g * deg C))	4.1868	3.997
Blood Flow Rate (g/(cm ³ * s))	0	
Refractive Index (n)	1.33	
RPE	Mainster	DeMarco
Thermal Conductivity (J/(s * cm * deg C))	0.00628	0.00565
Specific Heat (J/(g * deg C))	4.1868	3.68
Blood Flow Rate (g/(cm ³ * s))	0.001	
Refractive Index (n)	1.33	
Choroid	Mainster	DeMarco
Thermal Conductivity (J/(s * cm * deg C))	0.00628	0.0053
Specific Heat (J/(g * deg C))	4.1868	3.84
Blood Flow Rate (g/(cm ³ * s))	0.001	
Refractive Index (n)	1.33	
Sclera	Mainster	DeMarco
Thermal Conductivity (J/(s * cm * deg C))	0.00628	0.0058
Specific Heat (J/(g * deg C))	4.1868	4.178
Blood Flow Rate (g/(cm ³ * s))	1.00E-12	
Refractive Index (n)	1.33	

does not illicit a comparable reaction because the laser energy is not visible, requiring a longer aversion response time. Simulation parameters are based off Mainster eye model (except where DeMarco parameters are explicitly noted) using the Arrhenius Rate Process Model

$$\Omega(z, r, t) = A \int_0^t \exp^{\frac{-E_a}{RT(z, r, t)}} dt \quad (3.5)$$

where A and E_a are the tissue-dependent constant of integration and activation energy, respectively, R is the gas constant ($8.314 J/^\circ K mol$), T is the temperature ($^\circ K$) as a function of z, r and time, and Ω is the value of the normalized Arrhenius damage integral. In a one-dimensional simulation, the source term is determined as a spatially averaged irradiance (W/cm^2) along the z -axis. In a two-dimensional simulation, the source term is solved using the cylindrical coordinate space in the propagation direction, z , and radial direction, r , using a user-defined beam profile.

Figure 3.4 shows the three-dimensional simulation space using a two-dimensional simulation with radial symmetry. Damage is predicted in the numerical simulation when the normalized Arrhenius damage integral is greater than 1. In the case of a threshold search simulation, convergence on the damage threshold is defined to be the emitter power required for the damage integral to reach $1 \pm \epsilon$, where ϵ is a user-defined percentile tolerance parameter defined to be 0.03 in this study.

Simulated exposure thresholds are calculated at the retina and must be transformed to account for transmission loss in order to be compared to similar experimental data for validation using findings of Maher[22]. Furthermore, since this modeling effort is to account for human variance, experimental data must also be normalized to account for rhesus-to-human variance using a factor of 1.765 [28]. Analysis of the results to show the influence of varying factors follows.

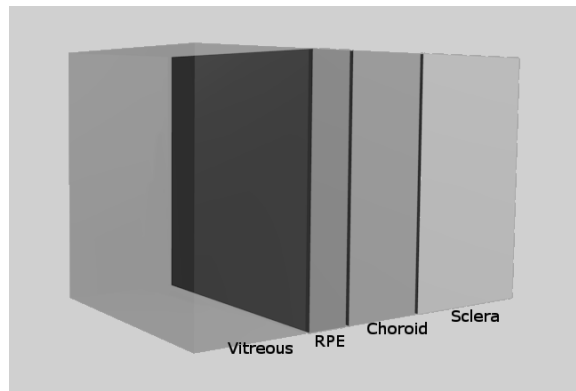


Figure 3.4 Figure depicting retinal layering system used in BTEC Thermal Model simulations. Grid resolution and sizing may be varied dependent on input beam characteristics.

3.5 Results

MATLAB is used to create 50,000 eyes based on revised covariance data. The critical input parameters are verified to come from normal or near-normal distributions. Due to the population and variates, there are some cases (generally $< 3\%$) in which the retina spot size is smaller than the assumed diffraction limited spot size

of 10- μm and are discarded. Their probability is redistributed over the remaining variates. The remaining population is compared to the Rozema results with excellent agreement (Table 3.2). These results are also compared to a mean spot size of 124- μm for visible light[31] representative of a -1 diopter mean refractive error for human eyes[29](model predicts a mean spot size of 127- μm). The results are processed with the Rockwell ABCD ray propagation code to determine spot size and distribution of spot size (Figure 3.5).

Table 3.2 Comparison of Rozema[29] data, Rozema Model, and proposed model. Proposed model output matches data and previously published results.

Eye Model Results - Right Eye Mean (StDev)						
	Rozema Data		Rozema Model		Revised Model	
Age	-	-	39.878	(12.20)	39.849	(12.183)
Anterior Keratometry (D) - K_A,M	-	-	43.294	(1.360)	43.295	(1.356)
K_A,J0	-	-	0.297	(0.280)	0.299	(0.281)
K_A,J45	-	-	0.060	(0.230)	0.060	(0.229)
Ant Corneal Eccentricity	-	-	0.403	(0.175)	0.404	(0.175)
Posterior Keratometry (D) - K_P,M	-	-	-6.265	(0.220)	-6.265	(0.220)
K_P,J0	-	-	-0.166	(0.070)	-0.166	(0.070)
K_P,J45	-	-	-0.003	(0.060)	-0.003	(0.060)
Post Corneal Eccentricity	-	-	0.151	(0.280)	0.150	(0.280)
Radius Curvature - Lens Ant (mm)	10.427	(1.40)	10.370	(1.40)	10.436	(1.403)
Radius Curvature - Lens Post (mm)	-6.864	(0.850)	-6.850	(0.90)	-6.869	(0.850)
Lens Thickness (mm)	4.070	(0.350)	4.150	(0.570)	4.071	(0.350)
Cornea Thickness (mm)	0.545	(0.032)	0.546	(0.035)	0.545	(0.032)
Anterior Chamber Depth (mm)	2.870	(0.380)	2.850	(0.390)	2.870	(0.379)
Axial Length (mm)	-	-	23.667	(1.120)	23.668	(1.119)
Pupil Size (Scotopic)	6.505	(1.120)	6.470	(1.070)	6.502	(1.118)
Lens Power (D)	-	-	22.994	(2.140)	22.994	(2.140)
Vitreous Depth (mm)	16.150	(1.150)	16.210	(1.030)	16.183	(1.053)
Posterior Lens Surface Depth (mm)*	-	-	7.457	-	7.485	(0.414)
Anterior Lens Surface Depth (mm)*	-	-	3.307	-	3.415	(0.376)
Ratio - Axial Length/Ant Corn RC*	-	-	-	-	3.030	(0.140)
Radius Curvature - Cornea Ant (mm)	7.810	(0.250)	7.820	(0.240)	7.829	(0.520)
Ratio - Ant Corn RC/Post Corn RC*	-	-	-	-	1.210	(0.045)
Radius Curvature - Cornea Post (mm)	6.440	(0.230)	6.450	(0.220)	6.477	(0.495)

* Denotes values not published by Rozema - Calculated from results or other sources

Computer simulations using the BTEC thermal model are used to examine how the effects of spot size impact damage thresholds upon the retina. Retinal spot sizes are taken from the empirical cumulative distribution function of the eye model results

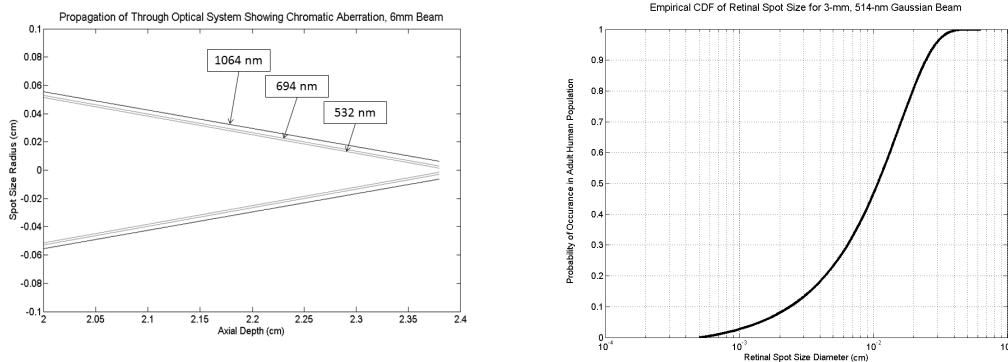


Figure 3.5 Graphic showing effects of wavelength on spot size as a function of axial depth (left) and the CDF of spot size as determined by Rockwell ray trace model for a 3-mm, 514-nm laser exposure (right).

corresponding to the 1-, 5-, 10-, 16-, 25-, 50-, 75-, 84-, 90-, 95-, and 99-percentiles. The BTEC thermal model predicts damage thresholds corresponding to these retinal image sizes and the resulting thresholds are mapped to a cumulative distribution function to estimate the probability of damage based on biological variance in eye focal geometries, wavelength, and exposure duration. Results are compared to trends in experimental data normalized for transmission and species differences (Figure 3.6).

Table 3.3 Table of 0.1- and 1.0-second results. Higher probit slope values indicate smaller variance in threshold due to biological variance. MDLS (Minimum Diffraction Limited Spot Size) = 10 μm

3-mm Diameter Gaussian Beam at Cornea									
Probability of Occurrence	514-nm			694-nm			1064-nm		
	Retinal Spot Size (μm)	0.1-s Damage Threshold (μ)	1-s Damage Threshold (μ)	Retinal Spot Size (μm)	0.1-s Damage Threshold (μ)	1-s Damage Threshold (μ)	Retinal Spot Size (μm)	0.1-s Damage Threshold (μ)	1-s Damage Threshold (μ)
MDLS	10	81	680	10	153	1265	10	652	5282
0.16	40	257	2065	52	563	4359	65	2746	19481
0.5	110	739	5456	142	1581	10886	169	6732	38720
0.84	215	1663	10854	257	3288	19609	287	11802	57336
0.99	367	3547	19764	408	6363	32453	438	20565	84763
	ED84/ED50	2.249	1.990	ED84/ED50	2.079	1.801	ED84/ED50	1.753	1.481
	Probit Slope	2.840	3.347	Probit Slope	3.146	3.913	Probit Slope	4.102	5.865
6-mm Diameter Gaussian Beam at Cornea									
Probability of Occurrence	514-nm			694-nm			1064-nm		
	Retinal Spot Size (μm)	0.1-s Damage Threshold (μ)	1-s Damage Threshold (μ)	Retinal Spot Size (μm)	0.1-s Damage Threshold (μ)	1-s Damage Threshold (μ)	Retinal Spot Size (μm)	0.1-s Damage Threshold (μ)	1-s Damage Threshold (μ)
MDLS	10	81	680	10	153	1265	10	652	5282
0.16	71	461	3549	97	1048	7654	126	5187	31765
0.5	215	1669	10854	281	3691	21435	336	14365	65613
0.84	426	4477	23650	511	9077	42427	573	30864	113284
0.99	732	11200	48735	814	20249	79888	876	62840	197905
	ED84/ED50	2.683	2.179	ED84/ED50	2.460	1.979	ED84/ED50	2.149	1.727
	Probit Slope	2.333	2.956	Probit Slope	2.558	3.372	Probit Slope	3.011	4.216

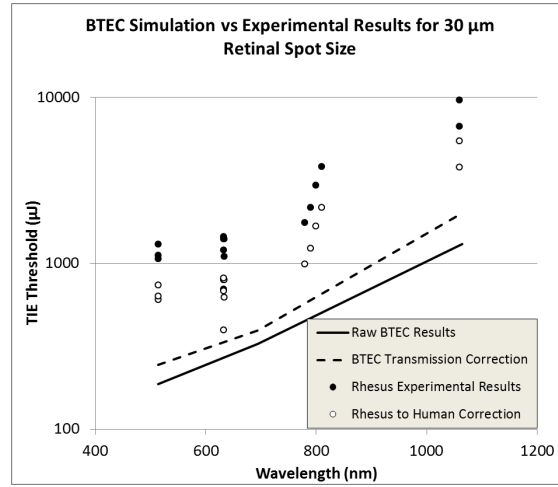


Figure 3.6 Graphic showing comparison of BTEC Thermal Model and experimental damage threshold results, raw data as well as data corrected for species variation and transmission loss. Slightly higher experimental threshold most likely due to laser beam scattering, rhesus to human conversion factor, or effects of anesthesia on subjects.

This same methodology is used to predict shifts in the damage thresholds in the cases of variance in thermal properties of the retina. The Mainster model uses thermal properties of water to simulate the retina and neighboring tissues. The DeMarco Model contrasts this approach by using the thermal properties of brain gray matter since both tissues are highly concentrated with neural cell bodies. Table 3.1 displays values used in simulation and Table 3.4 shows these results.

Table 3.4 Results from 694-nm, 0.1-s and 1.0-s simulations using both Mainster and DeMarco thermal properties. In both cases, thermal parameter variation of approximately 10% yields a similar shift in damage threshold.

Probability of Occurrence	0.1-s Mainster Threshold (μ)	0.1-s DeMarco Threshold (μ)	0.1-s Difference	1.0-s Mainster Threshold (μ)	1.0-s DeMarco Threshold (μ)	1.0-s Difference
MDLS	152	137	-9.9%	1265	1137	-10.1%
0.16	587	526	-10.3%	4359	3947	-9.5%
0.5	1606	1449	-9.8%	10886	9788	-10.1%
0.84	3296	2982	-9.5%	19609	17658	-10.0%
0.99	6414	5834	-9.0%	32453	29258	-9.8%

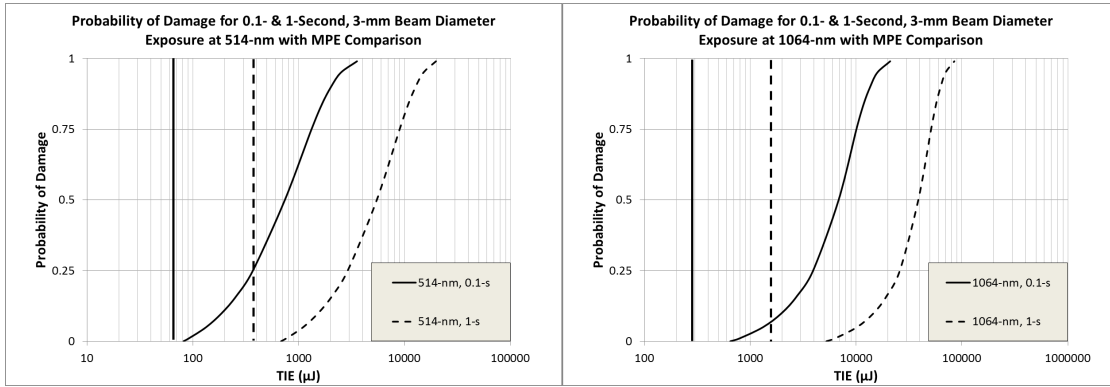


Figure 3.7 BTEC thermal model results for 6-mm beam at the cornea using only biological variance in focal geometry for 100-ms and 1-s exposures. Vertical lines represent Maximum Permissible Exposure (MPE) Limits for comparison.

3.6 Discussion

The results for threshold predictions are compared to experimental data. For validation, each simulated threshold is normalized to determine power at the cornea using a wavelength-dependent transmission loss coefficient. If an exposure is determined to have a threshold of $100\mu J$ but lost 10% during ocular propagation due to transmission loss, the normalized simulated threshold at the cornea is $110\mu J$. The experimental results, most often reported from experiments involving the Indian rhesus monkey, are also normalized as described by Rongjia[28]. In general, simulated thresholds are slightly lower than experimentally determined threshold values by a factor of about two to three. The higher experimental thresholds may be attributed to scattering of the laser energy by ocular media, anesthesia effects, or other parameters of simulation as well as interspecies differences not accounted for by a simple conversion factor published by Rongjia. However, the spread of data is the focus of this discussion.

The predicted damage threshold results show a sizeable threshold spread based solely on biological variance in focal geometries. As mentioned previously, a significant amount of retinal damage threshold studies fuels safety standards research. It is

therefore critical to compare current safe exposure limits to these modeled threshold values.

Table 3.5 Simulation predicted damage thresholds compared to current safe exposure limits for a 3- and 6-mm Gaussian beam. Table values are given as ratio of threshold/exposure limit. MDLS (Minimum Diffraction Limited Spot Size) = 10 μm

3mm Gaussian Beam Diameter					6mm Gaussian Beam Diameter				
Exposure Time (s)	Probability of Occurrence	Wavelength (nm)			Exposure Time (s)	Probability of Occurrence	Wavelength (nm)		
		514	694	1064			514	694	1064
0.1	MDLS	4.7	8.8	8.8	0.1	MDLS	1.2	2.2	2.2
0.1	0.01	5.2	10.1	10.4	0.1	0.01	1.5	3.0	3.1
0.1	0.50	42.4	90.7	91.3	0.1	0.50	23.9	52.9	48.7
1.0	MDLS	6.9	12.9	12.7	1.0	MDLS	1.7	3.2	3.2
1.0	0.01	7.8	14.8	14.8	1.0	0.01	2.2	4.3	4.4
1.0	0.50	55.7	111.1	93.4	1.0	0.50	27.7	54.7	39.6

Safe exposure limits are generalized to be a fraction of the experimentally determined ED_{50} values. The simulated thresholds determined by varying focal geometries generally fall lower than those found in experimental work by a factor of about two to three. However, it must be noted that larger beams at shorter wavelengths are uncomfortably close to existing safe exposure limits even considering the slight difference between the simulated and experimental thresholds. From Table 3.3, the simulated damage threshold for a 6-mm, 514-nm exposure at 0.1-seconds based on a 50% probability of occurrence is 1669 microjoules. For the same exposure, the 1% probability of occurrence threshold is 104 microjoules. This is approximately one-sixteenth of the simulated ED_{50} value. On the other hand, the simulated 3-mm, 694-nm exposures at 1-second is 10,886 microjoules. The 1% probability of occurrence threshold is estimated to be 1,447 microjoules, one-seventh of the 50% threshold. While these thresholds may need to be adjusted somewhat to match experimental data points, it indicates that a fixed fractional safety cushion may not be appropriate for all wavelengths and exposure durations. Furthermore, these results are based on biological variance of the focal geometries and nothing more. By varying other non-convarying (independent) factors, the tails of the distribution would be further skewed. Therefore, it is important that each source of variance

is understood and well-modeled before safe exposure limits can be determined to minimize over- and underestimation of risk. Such errors can create unreasonably high or low exposure limits thereby creating a chance of injury or simply impeding laser research and development efforts.

Variance in thermal properties of the retina also affected thresholds but on a smaller scale. Specific heat is measured in terms of $\frac{J}{g \times ^\circ C}$ while thermal conductivity is given by $\frac{J}{s \times cm \times ^\circ C}$. The Arrhenius rate process model (Eqn 3.5) predicts damage based on a given time-temperature profile. A predicted threshold is given in terms of Joules, Joules per second (Watts), Joules per unit area (radiant exposure), or Watts per unit area (irradiance). The specific heat is related to threshold in a strictly one-to-one function since a 10% decrease in the amount of energy required to change the time-temperature profile creates a 10% lower damage threshold. Thermal conductivity introduces a time-dependency so this may be more influential for some exposure times than others. However, the results of this study indicate a negligible difference between the threshold percentages of the Mainster and DeMarco models at 0.1- and 1.0-second exposure durations.

3.7 Conclusion

Our findings support that focal geometry and, to a lesser degree, thermal property variance are influential in damage threshold studies. An alternative approach to using a fractional safety factor based on ED_{50} values for determining safe exposure limits is to determine the underlying distributions of thresholds of factors relevant to damage thresholds. Models such as this may be refined to capture more parameters to provide first-principles models a better input configuration in order to produce more reliable results. The result is a deterministic model applied to a probability distribution realized from a population.

It is clear from these results that the degree of spread of damage thresholds across a population varies with wavelength and exposure duration. Although it

may be difficult to characterize each distribution by each permutation of wavelength and exposure time, it is critical for quality safe exposure limits. Probabilistic risk applications could use this approach to describe an exposure as having a P^{th} percent probability of injuring a bystander.

In preparing for this paper, we came across other biological factors to consider for retinal damage threshold modeling but they were rejected in order to manage the scope of the effort. These include age, RPE cell density, and lens quality. Time-dependency should also be considered to examine how these affect thermal and mechanical damage thresholds. Ultraviolet wavelengths (200-400 nanometers) may also be considered with respect to biological variance to examine how the results change when the significance of thermal property variance is altered due to corneal absorption.

Lastly, it is important to mention that this work would not have been possible without the assistance of several people. Drs. Robert Thomas and Benjamin Rockwell, Air Force Research Laboratory, Human Effectiveness Directorate, Directed Energy Bioeffects Division, Optical Radiation Branch. These gentlemen supported this effort from the beginning with papers, notes, working models, and endless assistance. The authors would also like to mention the assistance of Dr. James Stringham and Mr. Gary Noojin from TASC, Inc. Their assistance and discussions helped to form the approaches used in this research with respect to modeling the sources of variance. Additionally, we would like to thank Dr. C. D. Clark, III, of Fort Hays State University, Hays, Kansas, for providing input for the BTEC configuration files. Finally, we would like to thank Dr. Jos Rozema of the Department of Ophthalmology at the University Hospital Antwerp for providing the eye data used in his research. A great deal of this work is based on his approach to modeling a random, covarying vector of eye parameters and his support is greatly appreciated.

4. Biological Variance-Based Dose Response Model for 514 to 1064 Nanometer Laser Exposures

4.1 Abstract

Emerging directed energy systems promise to provide alternative engagement capabilities not bound by the limits of traditional kinetic munitions. However, doctrine for directed energy engagements largely remains under development. Further development of this doctrine requires a more complete understanding of effectiveness, weaponeering, and collateral effects. Collateral effects of laser systems must account for laser-tissue interaction effects for the eyes and skin. This is a complicated effort that requires more than a single endpoint for exposure limit due to the biological variance of potential bystanders. This research examines a probabilistic model for retinal damage caused by direct and indirect exposures to laser energy.

4.2 Introduction

Current and future laser systems provide scalable effectiveness across a variety of battlefield engagement types. Every year, research yields new applications for laser technologies that replace or supplement traditional kinetic engagement tactics or enhance capabilities to perform missions never before carried out. Additionally, many military operations conducted today using traditional kinetic weapons benefit from laser technology. Low-power, man-portable systems are used to create non-lethal glare effects to alert or deter non-combatants. Laser-kinetic hybrid systems such as those used in some precision guidance munitions benefit from the precision of lasers to strike targets with unprecedented accuracy. Future technologies such as megawatt-class, aircraft-based systems have already been proven in live-fire demonstrations to successfully destroy ballistic missiles in flight with better accuracy and speed than a kinetic system could achieve. Future directed energy system applications will certainly exceed today's expectations and current imaginary bounds.

The promise of line-of-sight, speed-of-light engagements that can strike anything resolvable by the optics is of high interest. The ability to disrupt a sensor or disable a vehicle without explosive fragmentation often experienced in kinetic engagements will reduce the probability of injuring non-combatant personnel or unintentionally destroying civil assets. The reduction in collateral effects of high-power laser systems provides a subjective rationale for directed energy research. However, for such a comparison to be made objectively, the severity of the collateral effects for both types of engagements must be quantifiable. Kinetic weapons assess risk of collateral effects using a risk-based approach to probability of injury due to aiming error, fragmentation, and explosion. It is critical to determine a risk-based method for laser systems to make an objective comparison. Dose-response models for directed energy are an example of such a tool.

High-power engagements are not the only area requiring risk assessment methodology. Risk assessment methods will benefit the development and deployment of low-power emitters used in glare systems. Glare systems, also known as laser dazzlers, are limited by maximum permissible exposure (MPE) limits and associated nominal ocular hazard distance (NOHD) that were developed for the laboratory and industry, not for the combat environment. The MPE is based on analysis methods that combine all statistical variance from experimental work into a safety factor high enough to eliminate any chance of retina injury. However, experimental variance comes from equipment quality, researcher capability, and biological variance of the research subjects. To truly understand risk to human subjects, the focus must be placed on biological variance while reducing the influence of the other sources.

This research details a method to create a probabilistic model based solely on biological variance to assess risk of retinal damage caused by unintended high-power laser reflections and low-power glare systems. This research can provide a framework for future analyses efforts in the direction of developing decision support tools. Damage thresholds are simulated using the BTEC Thermal Model[15] based

on the probabilistic output of the eye model previously developed by Wooddell et al.[42]. Statistical methods are applied to create a more robust tool for accommodate exposures from 10-milliseconds to 1-second for wavelengths between 514 and 1064 nanometers. This research can assist decision-makers and researchers to effectively create doctrine, tactics, techniques, and procedures for military and non-military applications

4.3 Background

ANSI Z136.7 [1] sets the guidelines for safe industrial and laboratory laser use. These guidelines were created based on decades of experimental damage threshold data supplemented with theory and modeling and simulation data. The experimentally determined damage threshold is often defined as the amount of energy required to create a minimal visible lesion (MVL), often on the order of 10 to 20 micrometers in diameter, on the retina. The reported thresholds may vary from experiment to experiment as a result of biological variance within the sample populations, measurement error from one laboratory setup to the next, damage threshold observation methods or definitions, and uncertainty stemming from either device precision or unknown factors. The biological variance in the focal geometries of the eye is also significant source of variance in damage thresholds [42]. The addition of the other factors mentioned above creates the need for a large safety cushion in order to ensure complete safety in these industrial and laboratory settings.

Lasers used in a military operational capacity follow the same safe exposure limit guidelines set for industrial and laboratory research. Laser dazzlers, relatively low-powered emitters used to warn or cause temporary vision impairment, are designed to expose targets at levels less than the safe exposure limit. In 2005, the Marine Corps emphasized the value of this technology by citing laser dazzlers as an urgent need [12], formally requesting expedited delivery of dazzler systems to increase stand-off distances, safeguard civilians, and diffuse situations in danger of

escalation. Systems such as the B.E. Meyer Glare MOUT can be mounted on vehicles in convoy operations and directed towards other vehicles that impede the convoy's progression. Checkpoints employ laser dazzlers to act as a signal to oncoming traffic to slow down or stop [35, 25]. Washington, D.C., employs a relatively large dazzler system to visibly warn aircraft flying into restricted airspaces. Dazzler systems such as these are effective tools for night-time operations but lose much of their effectiveness during the day due to the limited amount of power that can be delivered to the target that has a much smaller pupil as a response to the daylight. Each of these systems mentioned above are intended to be used in situations where lives may be at stake and, therefore, the need for successful engagements may warrant a small risk of injury.

Understanding the underlying dose-response relationship between laser energy and retinal injury enable the creation of models that can help decision-makers develop doctrine and expand application of directed energy technologies. A risk-based assessment methodology for military laser applications would improve the overall quality of trade space analyses for laser system deployment. To develop such a model, the statistical distributions of damage thresholds for a population must be classified in order to separate biological variance from the other factors associated with error or uncertainty.

These distributions of damage provide insight to damage thresholds for a given cumulative probability. Not only will a better understanding of the damage threshold distribution allow safety margins to be applied in an optimal fashion, it will allow decision-makers to have a means of allocating an increased risk when the benefit in troop safety is required. For example, a policy may dictate that effective dazzler use during nighttime hours is possible under the safe exposure limit restrictions of the ANSI Z136.7 but daytime engagement requires a power level that exceeds the limit for effective use. Using the statistical eye model developed by Wooddell et al., a 532-nm daytime exposure (3-millimeter pupil diameter) with an aversion response time of

100-milliseconds has a probability distribution based on focal geometry that results in a 12-micrometer diameter spot on the retina with a probability of 1%. The predicted damage threshold measured in total intraocular energy (TIE) for such an exposure is approximately 5.2 times higher than the exposure limit. In other words, increasing laser emitter power by 520% suggests only damaging 1 individual out of 100. The daytime effective energy may be only slightly higher than the safe exposure limits but having a probabilistic model to examine the trade space between effectiveness and safety is invaluable.

The above example shows how probabilistic retinal damage modeling can assist on the battlefield through the use of laser dazzlers in non-life threatening situations. However, the effective use of laser dazzlers can also assist in the United States in civil applications. The Washington, D.C., laser dazzler system is meant to be a first layer of defense when communication or navigation mistakes occur. Rather than immediately launching fighter aircraft over one of the nation's busiest cities to *escort* the violating aircraft away, the authorities use the laser system to signal the aircraft. During hours of darkness, these lasers are easily seen. However, during the daylight hours, they appear less bright and may not be noticed in a timely manner. The risk-based approach to using this laser system would likely allow the perceived intensity of the laser to be increased by a substantial factor, improving the success rate of daytime warnings with minimal impact on safety. These systems are extremely important due to the sheer number of potential threats requiring a fighter response. Between September 11, 2001, and May 17, 2009, fighter aircraft responded to more than 2,100 possible threats over the United States and carried out more than 51,000 missions in support of the overall air defense effort [18]. Improving the performance of these systems may help to reduce the number of aircraft launches in response to these threats in supported regions of the country.

Another need for such risk assessment tools for laser systems comes from applications where eliminating the possibility of direct or indirect exposures at a safe

exposure level cannot be eliminated. For example, the United States government owns several thousand square miles of land suitable for testing directed energy systems used as target designator and guidance systems. Range certification for the use of directed energy systems requires an assessment of the NOHD for each target area. The NOHD is a distance calculated from the laser source or target to account for direct or reflected laser power density transmission loss through the atmosphere. The NOHD is the distance the laser energy must travel before it is less than the maximum permissible exposure (MPE) limit as defined by the ANSI Z136.7. Certification is granted for those ranges where the entire risk can be mitigated, usually by restricting flight paths for laser system engagements and by closing off access to several dozen square miles of land for the duration of testing. In the US, this practice produces no disruptions to the public due to the sheer size of the test ranges.

However, in countries such as the United Kingdom (UK), the land mass is much smaller although their collaborative endeavors into laser research with the United States enable them to possess many of the same technologies. Researchers at the Air Force Research Laboratory are working with the UK Ministry of Defense (MoD) to adopt a new methodology for military laser risk assessments. Current deterministic safety models ensure there is a zero chance of injury from a laser exposure but at an extremely high cost in testing area. The probabilistic approach to risk assessment accepts an extremely low probability of damage for the benefit of a lower cost in terms of land area restrictions. Therefore, the probabilistic approach aims to resolve the need to prohibit access to large parcels of land for laser use at the cost of a risk equivalent to the laser-system equipped aircraft itself suffering a catastrophic accident. The underlying probability of laser injury, however, assumes a distribution of damage drawn from dose-response models based on experimental results using probit analysis [9]. Probit analysis results include the effects from biological variance but also negatively affects any probabilistic model due to the inclusion of factors that cannot be removed, such as measurement error or observer agreement. Wooddell et

al.[42], as well as other independent research efforts [34, 31], show evidence that this method of probabilistic modeling is a poor approach due to the area of interest being in the tails of the distribution. This is an artifact of using a lumped variance approach such as probit and can be resolved knowing the details of the underlying biological variation's impact on damage threshold.

Another application of dose-response models is in the development of collateral effects decision-support analysis tools. These tools allow decision-makers to estimate the risk of injury to bystanders during a high-powered laser engagement. Invisible lasers such as the neodymium-doped yttrium aluminium garnet (Nd:YAG) operating at a wavelength of 1064 nanometers are ideal for use in relatively higher powered systems. According to Boeing, the major defense contractor responsible for the development of the Airborne Laser (ABL), the Nd:YAG laser on the testing platform produced approximately 1,000 watts. This laser is used as the beacon illuminator laser to measure optical distortion on the propagation path caused by turbulence or atmospheric effects. Once this high power beam illuminates a target, it is either absorbed or reflected. The study of where the reflected energy lands and how it may affect bystanders is an example of laser collateral effects analysis.

Collateral effects decision-support tools sample the elliptical footprint of the Nd:YAG's energy reflected by the target cruise missile onto the Earth's surface. The surface spot is represented by a discrete grid with associated laser beam characteristics that account for power loss from atmospheric transmission and absorption. The dose-response model uses each grid point's power level as input and returns a probability of damage based on user-defined criteria. Figure 4.1 shows the difference between using traditional deterministic hazard distances and using a probabilistic approach. Note that the probability of injury is based solely on the assumption of looking directly at the beam; however, it may be used in conjunction with a behavioral model that estimates the probability of direct viewing. The two probabilities can then be evaluated, with equal or unequal weightings, to determine the proba-

bility of injury for any given engagement scenario. This estimated risk is then used in the development of doctrine, tactics, techniques and protocols for the use of the ABL.

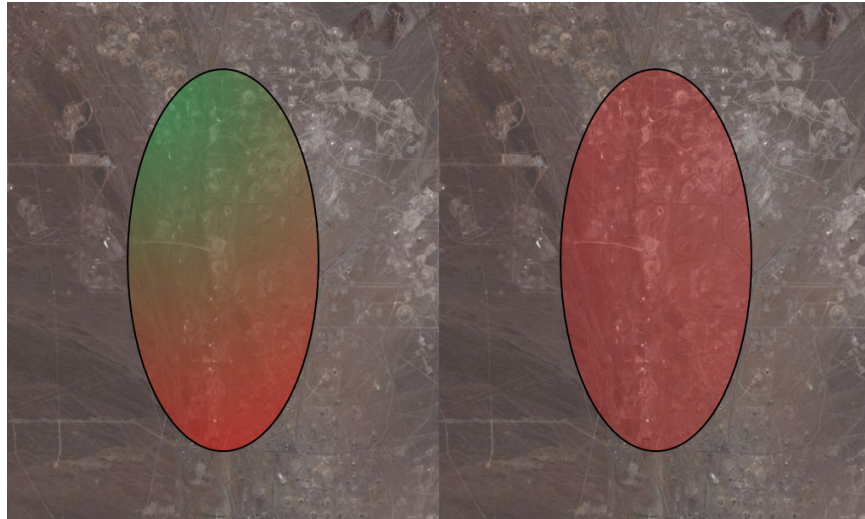


Figure 4.1 Graphic showing comparison between a deterministic and probabilistic approach to risk modeling. The probabilistic model (left) shows a color-coded degree of risk based on a Gaussian footprint of laser energy. The deterministic approach (right) shows only a region of unsafe exposures. Calculations for elevations are excluded from this example for simplistic demonstration.

The inclusion of the ABL system is for demonstrative purposes in the following sections, as the ABL program remains an unfielded, although extensively tested, laser system. The Nd:YAG system used by the ABL is also a pulsed laser system, not a continuous wave emitter. The pulses in the system under development are assumed to be much shorter than the time domain of this model but this example assumes a continuous wave emitter with the same time-averaged power of one kilowatt. Dose-response models for pulsed emitters function in a similar fashion.

Finally, another application that may benefit from a probabilistic approach to retinal damage modeling applies to a much broader population than those who may see a battlefield or fly aircraft in or near restricted airspace. Lasers are used throughout the field of medicine, especially for non-invasive imaging of human tis-

sues. Optical coherence tomography (OCT) uses photons emitted from a laser to paint a three-dimensional picture at a resolution of close to one micrometer [13, 39]. At this resolution, OCT is often able to detect diseases and injuries of the human eye.

Resolution and imaging at the retina's surface is at the sub-cellular level but diminishes with depth due to laser propagation effects. Laser energy is absorbed, transmitted, reflected, and scattered as it propagates through a medium. The eye's focal path transmits most of the photons at OCT wavelengths but the retina acts as a strong absorber decreasing the signal-to-noise ratio of the OCT device decreasing image quality. According to Schmitt [30], OCT imaging performance depends on emission in the near infrared, short temporal coherence length, and high irradiance. The first and third aspects are directly examined in this study. Wooddell et al. show that near infrared wavelengths had a much steeper slope in the cumulative distribution function suggesting that the safety factor built into safe exposure limits may be reduced without introducing unnecessary risk. This in turn would allow an increased irradiance (emitter power) and, ultimately, better sub-retinal imaging with no significant increase in risk. Furthermore, a probabilistic approach to damage may even allow for the introduction of minimal risk in cases where better imaging is critical to the patient's health.

Statistical variance in threshold studies plays a significant role in directed energy biological effects, or *bioeffects*, research. Generally, inter- and intra-subject variations guarantee a range of damage threshold values rather than a single experimental endpoint. These ranges are reported using descriptive statistics, typically a mean and a measure of variance that describes the spread of the data. Determining the degree of influence for each source of variance in damage threshold studies is a crucial factor in determining a population's damage threshold characteristics. Understanding the root causes of threshold variance is important in the development of safe exposure limits because many aspects used in their determination is based on a

probabilistic approach. This research focuses on the influence of biological variance in focal geometry of the human eye across a population and applies the distribution of geometric parameters to create a dose-response model.

Dose-response models for laser exposures are not a new concept. However, the underlying probability distributions sampled for the responses vary drastically. Schulmeister et al. produced a space-based laser probabilistic risk analysis model for retinal injuries based on the probability of exposure at any given time [32]. This study agreed with the Sliney study [34] that probit analysis slope values could not be used as a means to calculate probability of damage, especially in the tails of the distributions. Therefore, Schulmeister adjusted the probit slope values to account for biological variability and experimental difficulties such as achieving a minimal spot on the retina 20 micrometers in diameter.

Another dose-response model was developed in 2008 by the United States Air Force Research Laboratory (AFRL) [2] for exposures at 1064 nanometers. This model was based on a modified least squares fit over a time domain ranging from 1 microsecond up to 1,000 seconds. The model predicted a mean dosage that created a minimal visible lesion but reduced the results by a small fraction to keep approximately 90% of all experimentally determined damage thresholds above the model output. This was done to prevent underestimating risk. Then, the ANSI-defined safe exposure limit served as a lower bound occurring four standard deviations less than the mean in log-scale such that

$$\log_{10}(\mu_t) - \log_{10}(MPE_t) = 4\sigma \quad (4.1)$$

$$\sigma = \frac{\log_{10}(\mu_t) - \log_{10}(MPE_t)}{4} \quad (4.2)$$

where each μ_t is the time-dependent mean dose and MPE_t is the time-dependent maximum permissible exposure limit. Sampling from a normal distribution with a mean of $\log_{10}(\mu_t)$ and standard deviation σ resulted in the probability of damage for

a given dose. It could also be solved for the inverse distribution to determine the dose required for a specified probability. This inverse distribution effort was chosen after earlier research based on probit slope values calculated from the experimentally determined ED_{50} and ED_{84} resulted in extrapolation problems for longer exposure durations.

This 1064-nm model assumed only experimental variance for on-axis exposures. It was intended to be a means to assess risk of retinal damage for decision support and analysis tools built by AFRL. However, it suffers from a lumped variance approach rather than basing the distribution of damage thresholds off of a biological variance-based distribution of spot sizes and resulting power densities.

The current research effort creates the basic underlying distribution that may be sampled by a behavioral model similar to the approach by Schulmeister et al. described above or used as a library for decision support and analysis tools.

4.4 Method

The goal of this research is to create a baseline model that can easily be implemented in analysis applications in the form of a library or executable file. This research effort uses the results described by Wooddell et al.[42] using biological variance in focal geometry as the foundation for generating the probability distribution of damage for a given exposure duration and wavelength. The results generated by the statistical eye model agreed well with the human data; however, an experimental validation effort should be conducted to ensure the quality of the results for the statistical eye model as an input to the ray trace propagation and BTEC thermal model. This research effort assumes the results are representative of a human population and outlines the method to create a probabilistic dose response model for retinal damage.

The dose response model must accept laser beam parameters as input values. Characteristics such as exposure time, beam diameter at the corneal surface, and

wavelength are significant factors in determining retinal damage and are included as inputs. In order to get a probability of response, where the specific response is defined as a minimum visible lesion (MVL) caused by photothermal damage to the retina, laser emitter power must also be included as an input. However, if one was seeking to determine the emitter power associated with a specific probability of damage, this probability value must be an input variable.

This model assumes direct illumination from a continuous wave laser emitter onto the retina in the macular region. The macula is the center of the retina where central vision occurs. The areas outside of the 5-mm macular area is known as the paramacular region, the area responsible for peripheral vision. The paramacular region is much less sensitive and has been documented to have a laser damage threshold 40% higher than the macular region. Future studies may account for damage across all regions of the retina but this research assumes an on-axis exposure directly on the macula. Furthermore, this effort accounts for continuous wave exposures. Pulse train characteristics such as duty cycle and pulsewidth complicate extrapolation from this dose response model. However, dose response models may be created for a specific laser system if the pulse train characteristics are known similar to the method described in this paper.

The probabilistic dose-response model is dependent on damage thresholds estimated for a given exposure time, wavelength, and beam spot size on the retina. Spot size on the retina is a function of input beam diameter and wavelength for a randomly generated eye within a sample population. This population is generated as described by Wooddell et al. using a vector of parameter means and covariance matrix taken from the Rozema Statistical Eye Model [29] as well as a few other parameters from other data sets by Garner and Iyamu [11, 16].

After performing the spectral decomposition method of adjusting for missing data, the $k \times k$ covariance matrix, $\Sigma_{k \times k}$, is used along with the vector of means,

$\vec{\mu}$, to generate n random variates in k parameters. The built-in MATLAB function *mvnrnd* performs this task by

$$X_{n \times k} = N_{n \times k} \Sigma_{k \times k} + \mu_{n \times k} \quad (4.3)$$

where $N_{n \times k}$ is constructed from n variates in k parameters drawn from a random normal distribution. The product of $N\Sigma$ is the random error that is subsequently added to the mean value of each parameter contained in the vector $\vec{\mu}$. The matrix, X , contains most of the row vectors \vec{x} that are needed for input into the ray trace propagation model developed by Rockwell et al.[27]. However, the published Rozema data sample did not include each parameter necessary to perform ray tracing. The propagation distance through the anterior and vitreous chambers could be calculated from the data so these were introduced as new elements of \vec{x} . Radius of curvature was not a straightforward calculation from the Rozema data initially so ratio of eye length to curvatures from the other studies was used to estimate these parameters for ray tracing. It is important to note that this may have been the cause for a higher variance in these generated parameters than was observed in nature. This increased variance may skew the distribution in the upper tails. The lower tail of the distribution is fixed based on the diffraction limited spot size of 10-micrometers in this study. These new parameters were calculated using a mean and random error element following the Garner and Iyamu research.

The final matrix, X , consisted of $n = 50,000$ rows representative of a single eye possessing the parameters required for ray tracing. Ray tracing is modeled using the complex Gaussian beam propagation parameter to calculate the spot sizes in and out of each surface from the cornea to the retina as described by Rockwell et al.[27]. This relationship is defined by:

$$\frac{1}{q_i} = \frac{1}{R(z)} + i \frac{\lambda}{\pi w^2(z)} \quad (4.4)$$

$$q_f = \frac{Aq_i + B}{Cq_i + D} \quad (4.5)$$

where z is the propagation distance along the axis, q_i and q_f are the complex beam parameters in and out of a surface, respectively, and $R(z), w(z)$ are the radius of curvature and spot size (radius), respectively. $A, B, C,$ and D come from the ray matrix as

$$\begin{bmatrix} A & B \\ C & D \end{bmatrix} = \begin{bmatrix} 1 & d \\ 0 & 1 \end{bmatrix} \quad (4.6)$$

for propagation through a medium and

$$\begin{bmatrix} A & B \\ C & D \end{bmatrix} = \begin{bmatrix} 1 & 0 \\ \frac{n - n'}{Rn'} & \frac{n}{n'} \end{bmatrix} \quad (4.7)$$

for propagation at a medium change. The values n and n' are the prior and post medium refractive indices and R is the radius of curvature of the refracting surface.

The 50,000 spot size results are adjusted for diffraction limited spot size by removing m eyes with spot sizes calculated lower than this 10-micrometer diameter minimum. The probability for these relatively few points is redistributed among the remaining eyes.

Probability is assigned based on the empirical cumulative distribution function percentile scores. For a final adjusted sample population of $n' = n - m$, the 50th-percentile spot size is the spot size calculated for the $\frac{n'^{th}}{2}$ eye after the results had been sorted in increasing order. In general, the p^{th} -percentile spot is calculated for the $(n'/100)/p^{th}$ eye. For large populations, a search algorithm on the results of MATLAB's *ecdf* function simplifies this task.

These results are then used for input to the BTEC Thermal Model [15] to estimate damage threshold in terms of total intraocular energy in microjoules. Damage thresholds were sampled at 10-, 100-, and 1,000-millisecond exposure durations for spot sizes ranging from the diffraction limit of 10 micrometers up to 1000 micrometers and across multiple wavelengths that are classified as significant. Wavelength significance is based on local anomalies in absorption coefficients which result in sharp changes to damage threshold trends. The primary areas of interest are in the lower wavelengths between 500 and 650 nanometers and between 850 and 1000 nanometers where absorption behaved in a non-linear fashion.

The time, wavelength, and spot size dependent BTEC results are read into MATLAB to create surface approximations for each of the three exposure durations. Interpolation for the wavelength and spot size dependent damage threshold is performed for a given input vector on each of the three exposure time-dependent surfaces. Piecewise cubic Hermite interpolating polynomials (PCHIP) are used to interpolate the time dependent function sampled here in order to account for non-linear relationships between time and damage. PCHIP is used to ensure shape preservation for a non-constant Δt used in the interpolation. The MATLAB built-in function *pchip* performs this operation based on [10, 17].

This approach answers two primary questions for the dose-response relationship:

1. How much energy (dose) is required to cause a probability of damage for a given wavelength and exposure duration?
2. Given an exposure of a specific energy level, wavelength, and exposure duration, what is the probability of damage to someone exposed?

The following two sections describe how each question is answered using the model described above.

4.4.1 Estimating Dose for Probability of Damage. In order to predict dose required for a probability of damage, p , MATLAB is used to interpolate (cubic interpolant) a surface using three non-uniformly spaced data sets taken from exposure durations of 10, 100, and 1,000 milliseconds. Linear scaling of the threshold data measured in total intraocular energy (TIE) (microjoules) distributes the interpolation surface poorly so a log-10 transform is performed. Wavelength and spot size diameter is measured in nanometers and micrometers, respectively.

Consider a decision-maker that has determined the acceptable risk of damage for exposure to a green laser operating at 532 nanometers during the daytime to be 20% ($p = 0.20$). For this exposure, assume an aversion response time of 250 milliseconds. To determine the TIE threshold for this probability of damage, the model generates the surface from the BTEC simulation data for more than 300 time, wavelength, and spot size combinations. The first step is to calculate the retinal spot size based on cornea spot size and wavelength. This is done using the statistical eye model developed by Wooddell et al. The random seed used in generating the population may be toggled to reset each run or to begin the next run where the last run left off. The number of variates is also user-defined. Next, using the determined retinal spot size diameter, the damage threshold for the given exposure at 10 milliseconds is calculated. Figure 4.2 shows this as a point of interest.

Next, the threshold is calculated on the 100-millisecond surface and is repeated for the 1,000-millisecond exposure duration before the interpolation for time is performed. Figure 4.3 shows the points of interest on the three interpolated surfaces.

Finally, to calculate the threshold dose for an exposure duration between 10 and 1,000 milliseconds, the three previously determined, time-dependent thresholds are placed in a 3×2 matrix, $M_{3 \times 2}$, such that $M_{i,1}$ is time and $M_{i,2}$ is the associated damage threshold. The matrix is then input to the MATLAB PCHIP model. Figure 4.4 shows the interpolation and predicted dose to be 770.7 microjoules. It is important to note that adjustments must be made for transmission loss within the

eye since the predicted dose is determined to be the energy at the retina. These parameters are described by Maher in [22] and the procedure demonstrated in the following section for the inverse problem.

4.4.2 Estimating Probability of Damage for Dose. The inverse problem of calculating the dose required for a p^{th} -percentile probability of damage works similarly but in an iterative fashion. Given a dose, ED_X , and a tolerance, ϵ , the procedure described in the previous section is repeated until the power to achieve a specific probability of damage is within ϵ . The search algorithm is simple linear bisection on probability.

Consider the example in the previous section. The decision-maker has been told his laser system has an irradiance, measured in watts per square centimeter, of 0.06 at the estimated distance of corneal interaction. Using daytime exposure parameters that assume a 3-mm pupil diameter and 250-millisecond aversion response, total energy into the eye (dose) is calculated by:

$$Dose_{Cornea} = Irradiance\left(\frac{W}{cm^2}\right) \times PupilArea \times ExposureTime \times 10^6 \quad (4.8)$$

$$Dose_{Cornea} = 0.06 \frac{W}{cm^2} \times \pi\left(\frac{0.3}{2}\right)^2 (cm^2) \times 0.25(s) \times 10^6 \quad (4.9)$$

$$Dose_{Cornea} = 1060\mu J \quad (4.10)$$

After converting from joules to microjoules with a factor of 10^6 , the resulting energy at the cornea that can enter the pupil is 1060 microjoules. Finally, the decision-maker must account for transmission loss. This is performed using the transmission values

by wavelength as published by Maher [22] and is determined to be approximately 22%. The final power is determined to be 827 microjoules at the retina below.

$$Trans_{total} = Trans_{Cornea} \times Trans_{Aqueous} \times Trans_{Lens} \times Trans_{Vitreous} \quad (4.11)$$

$$Trans_{total} = 0.898 \times 0.988 \times 0.930 \times 0.947 = 0.78 \quad (4.12)$$

$$Trans_{Loss} = 1 - Trans_{total} = 0.22 \quad (4.13)$$

$$Dose_{Retina} = Dose_{Cornea} * Trans_{total} = 1148 \times 0.78 = 827 \quad (4.14)$$

Next, the dose-response model is used to estimate probability of damage from 896 microjoules at the retina. The result is found to be 0.219, 1.9% higher than the desired 0.2 probability specified in the example previously in section 4.4.1. However, the decision-maker may allow an increased risk over redesigning the laser emitter or adjusting utilization ranges to change irradiance at the cornea. If the 0.20 probability is a firm threshold, the decision-maker can use the results show in Figure 4.5 to adjust emitter parameters or utilization range.

4.5 Results

The foundation for this analysis is based on simulation data and must be validated through experiments prior to implementing such a dose-response model. This section assumes post-validation data is used to create the dose-response surfaces and that the retinal spot size probability distributions determined by the statistical eye model are representative of the human population.

Results are presented to show a contrast in ANSI-defined safe exposure limits by wavelength and exposure duration. This analysis will demonstrate these results in two cases. The first will examine nighttime and daytime trade space for a green 532-nm dazzler between a safe exposure and a 1% risk of damage. The second will examine an infrared (invisible) 1064-nm emitter for a one second exposure.

4.5.1 Trade Space for 532-nm Dazzler Systems. This first case examines a green dazzler system operating at 532 nanometers in both day and night time operating conditions. Daytime exposures will assume a limiting aperture (pupil size) of 0.3 centimeters in diameter. Exposures for the nighttime operations assume a wider aperture of 0.6 centimeters representing a pupil that has accommodated to the darkness in order to receive more light. Aversion response time in both cases is assumed to follow the ANSI-prescribed estimate of 0.25 seconds. Both cases also assume an on-axis exposure with macular illumination as opposed to paramacular (peripheral) illumination that may result in a much higher damage threshold.

In the case of a daytime exposure to the dazzler system, the maximum safe exposure limit at the cornea is calculated as follows:

$$MPE_{cornea} = 1.8t^{0.75} \times 10^{-3} = 6.36 \times 10^{-4} \quad (4.15)$$

This result is measured in radiant exposure ($\frac{J}{cm^2}$). To convert to power at the retina, a conversion to account for aperture size and transmission loss is as follows:

$$MPE_{retina} = MPE_{cornea} \times \left(\frac{A}{2}\right)^2 \times \pi \times 0.78 = 3.51 \times 10^{-5} \quad (4.16)$$

where A is the aperture diameter and 0.78 is the previously calculated transmission constant for 532-nm exposures. Finally, since the model uses power input as micro-joules, the result is multiplied by 10^6 yielding final power at the retina to be 35.1

microjoules. The same formula is applied to the 0.6 centimeter nighttime aperture resulting in 140.4 microjoules.

Next, increase radiant exposure while holding aperture conditions constant. Adjustments are made for limiting aperture and transmission loss for each radiant exposure level. The resulting powers are used as inputs for the dose-response model.

The model predicts radiant exposure at 644% of the maximum permissible exposure limit creates a 1% probability of damage for daytime exposures; however, a radiant exposure at only 180% of the maximum permissible exposure limit creates a 1% probability of damage for nighttime exposures. These are shown in Figures 4.6 and 4.7, respectively. These results suggest a need to investigate alternative approaches to exposure limits as daytime and nighttime vary so greatly due to pupil accommodation.

4.5.2 Collateral Risk Estimates for 1064-nm Emitter. Collateral effects decision-support tools allow decision makers to estimate the risk of injury to bystanders during a high-powered laser engagement. A typical ABL engagement would be to range, track, and focus onto a cruise missile in flight, making dynamic adjustments to propagation characteristics that are affected by atmospheric conditions. This example assumes the typical engagement scenario with the cylindrical body of the missile reflecting an ellipsoid back onto the earth's surface.

Collateral effects decision-support tools sample the elliptical footprint on the surface represented by a finite grid after estimating power loss from transmission and absorption. In turn, the powers are used as input to a dose-response model. The results of the model are then used to estimate the probability of injury should someone in the grid look directly at the laser beam. It is important to note that the probability of injury is based solely on the assumption of looking directly at the beam; however, it may be used in conjunction with a behavioral model that estimates the probability of direct viewing. The two probabilities can then be evaluated, with

equal or unequal weightings, to determine the probability of injury for any given engagement scenario.

The MPE limit for 1064 is calculated as above with an exception to aversion response time. Since this light is invisible, there is no uncomfortable stimuli until negative effects are induced. Therefore, the ANSI Z136.7 defines aversion response for invisible wavelengths to be an entire second. The one-second MPE for a 1064-nm exposure is given as $0.009 \frac{J}{cm^2}$.

Since pupil diameter is not wavelength dependent, aperture diameters for daytime and nighttime were the same as the previous example measuring 0.3 and 0.6 centimeters, respectively. Therefore, a radiant exposure at the MPE level yielded a daytime retinal power of 413.5 microjoules and nighttime retinal power of 1654 microjoules. The damage threshold for the assumed diffraction limited spot size of 10 micrometers is 5,280 microjoules. As the minimal spot size possible, this represents the 0th-percentile damage threshold. In other words, nighttime exposures can be up to 320% of the MPE limit while daytime exposures may exceed 1200% of the MPE limit before any possibility of damage occurs.

Figures 4.8 and 4.9 show the trade space for this exposure. Validation of this model is necessary but these results give strong indications that exposure limits should not only be based on wavelength and exposure duration, but also on time of day.

4.6 Conclusion

Dose-response models provide decision-makers with a foundation for decision-support analysis tools. The results of the examples show that dose-response models can be used effectively in the place of the deterministic safe exposure limits developed for industry and laboratory research. Decision-makers can use such models to quantify risk for many types of laser engagements from relatively low power dazzler systems up to supporting higher powered systems such as the Nd:YAG laser used on

the ABL platform. Additionally, future laser systems such as the ABL's megawatt-class chemical oxygen iodine laser that is used to shoot down the intended cruise missile targets once the Nd:YAG laser is used to adjust for distortions will undoubtedly need the same type of analysis performed although the operating wavelength of this system is not examined in this research.

The power range between the MPE limit and the p^{th} probability of damage is the trade space for the decision-maker. The information provided by dose-response models suggest the need for further analysis of daytime exposure limits enabling a higher emitter power for daytime dazzlers such as those used in restricted airspace. If an overall increase of the MPE limit is not desired, the results of a validated dose-response model could help to support a daytime waiver by the Food and Drug Administration (FDA), the approval authority in the United States for laser systems.

Waivers or MPE limit refinement will not only effect systems already developed. Dose-response models may be used to show no increased risk of injury during laser research experiments with respect to human subjects. A relatively new area of study called thermal lensing creates a visual distortion in the optical path of the eye using an infrared emitter. This is done by raising the temperature of the fluids through the absorption of the laser light, causing a change in the refractive index diverging the beams of focused light entering the eye. The result is a defocused image at the retina that cannot be resolved by the brain. Initial testing has shown this effect at current MPE levels although relaxing the exposure limits will benefit advanced applications of this phenomenon. Perhaps the coalignment of dazzler systems with a thermal lense inducing system may artificially scatter the visible wavelengths to disrupt a larger field of view. Increasing the exposure limits would allow for this added dazzler system's power since MPE is not calculated separately for a dual-beam system.

This study focuses on a few applications that may benefit from dose-response models. Other models developed for a wider time and wavelength domain present

new challenges but will be beneficial to the laser research community to include engineers, policy-makers, and end-users.

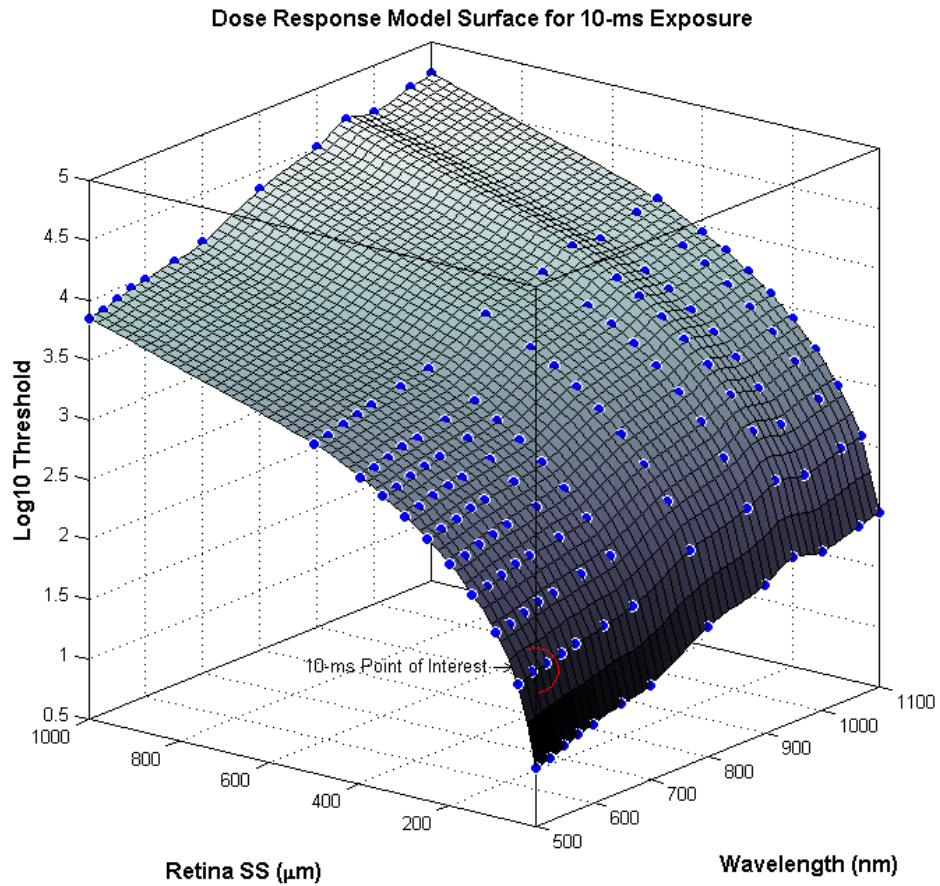


Figure 4.2 Surface generated from BTEC simulation data for 10-millisecond exposure. Point of interest on the surface in this graphic is the 20th-percentile (49- μm diameter) damage threshold for a 532-nm exposure calculated at 10 milliseconds. The plot displays the interpolated surface among the blue circles representing the simulated data.

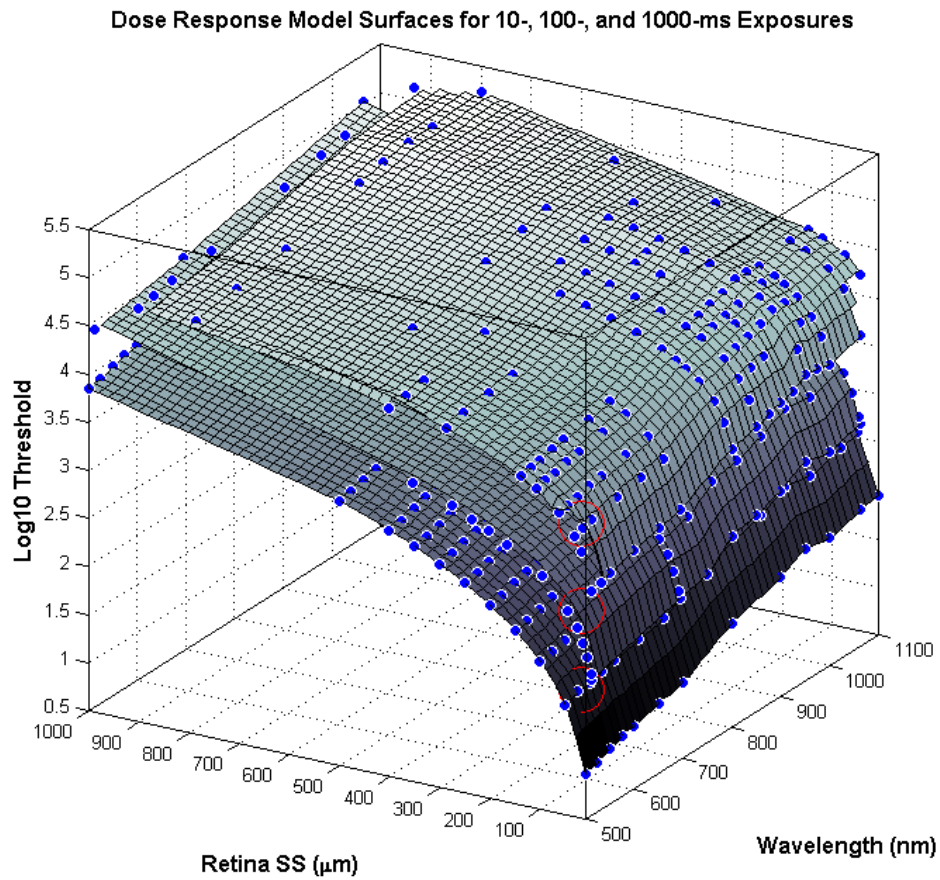


Figure 4.3 10-, 100-, and 1000-millisecond surfaces generated from BTEC simulation data. Point of interest for this example is the 20th-percentile damage threshold for a 532-nm corresponding to a 49- μm diameter retinal spot size. The plot displays the interpolated surfaces among the blue circles representing the simulated data.

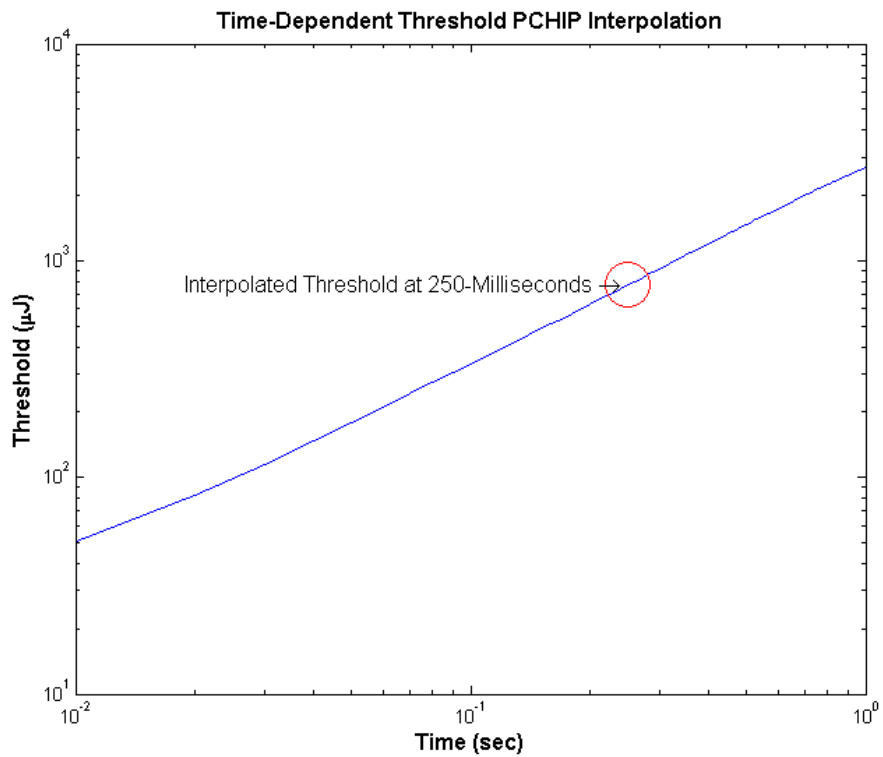


Figure 4.4 PCHIP model for time dependency. Point of interest is at 250 milliseconds with a TIE dose calculated to be 770.7 microjoules.

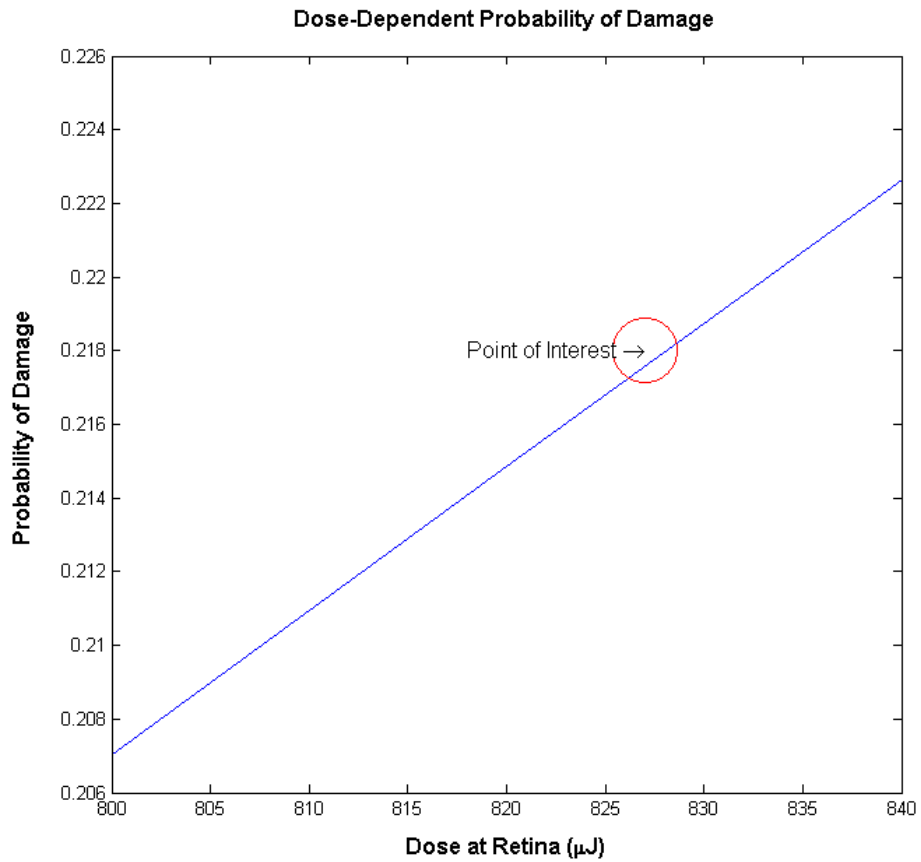


Figure 4.5 Probability of damage as a function of retinal dose and point result for example in this section. Plot visualizes trade-space for risk of dose between 800 and 840 microjoules.

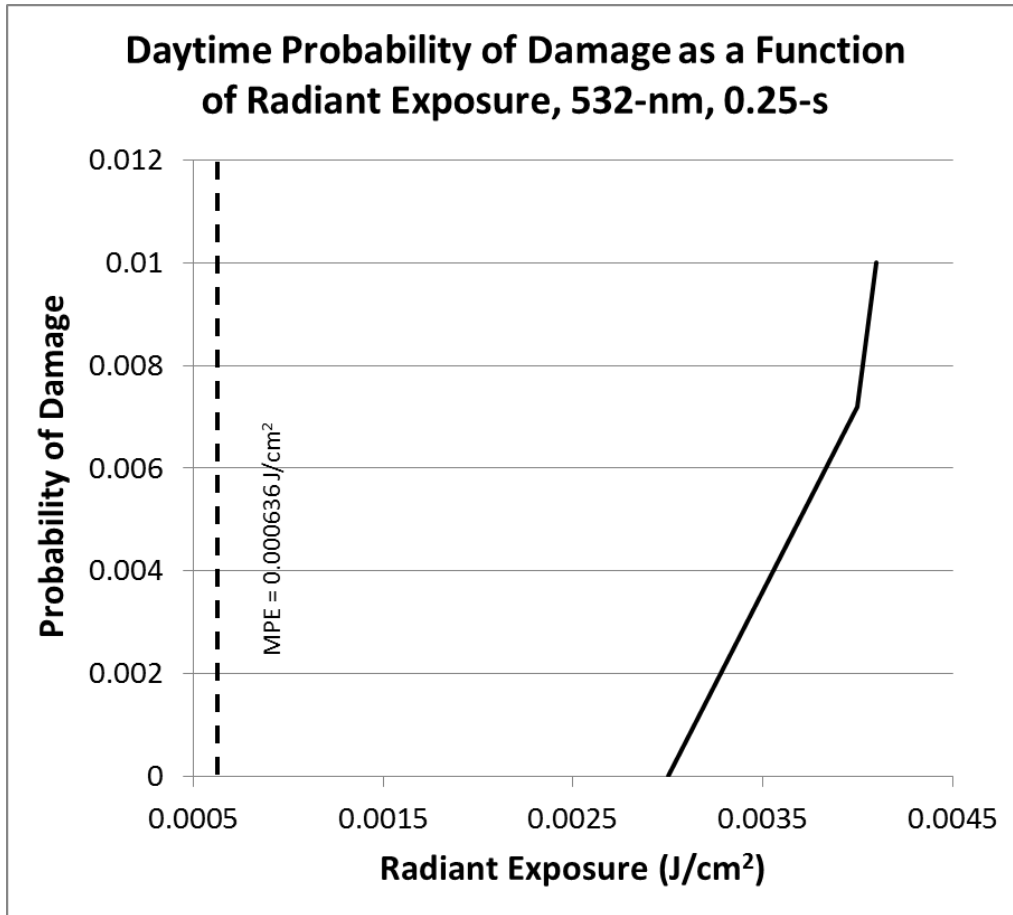


Figure 4.6 Plot depicting probability of damage as a function of radiant exposure for 0.3-cm pupil in daytime light conditions. Dashed line represents ANSI Z136.7-defined maximum permissible exposure (MPE) limit.

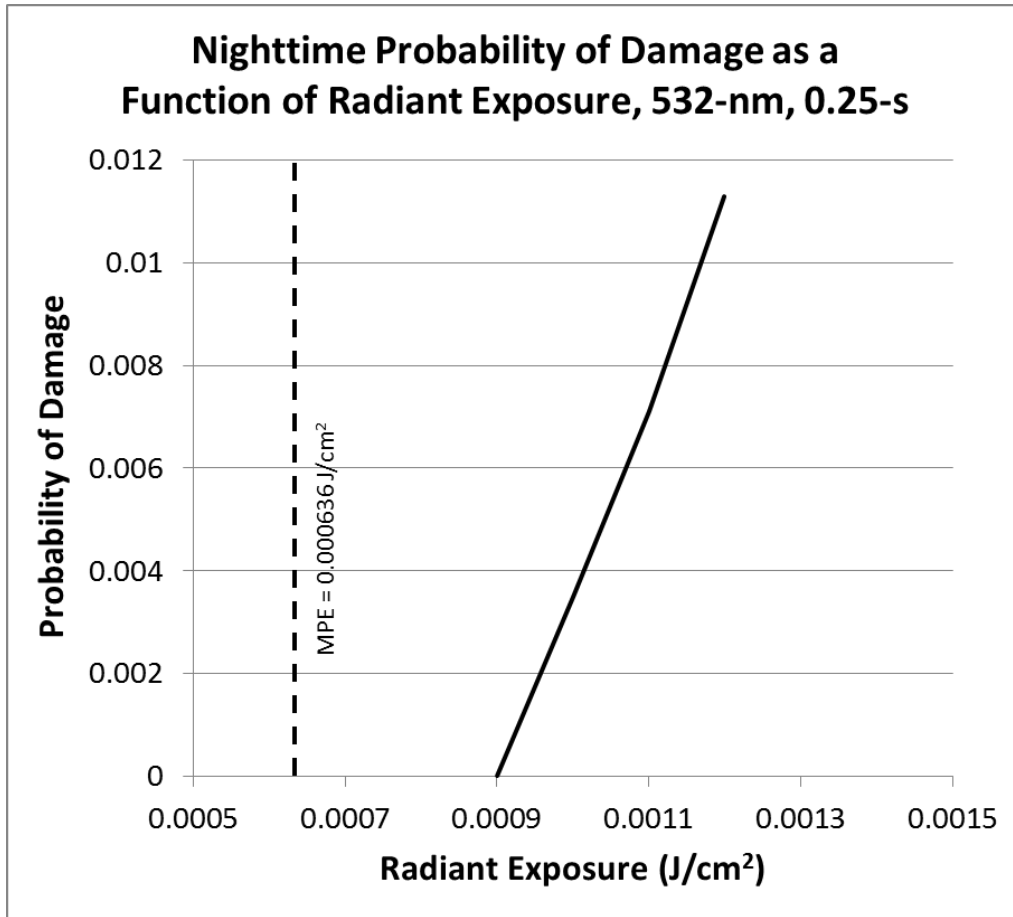


Figure 4.7 Plot depicting probability of damage as a function of radiant exposure for 0.6-cm pupil in nighttime light conditions. Dashed line represents ANSI Z136.7-defined maximum permissible exposure (MPE) limit.

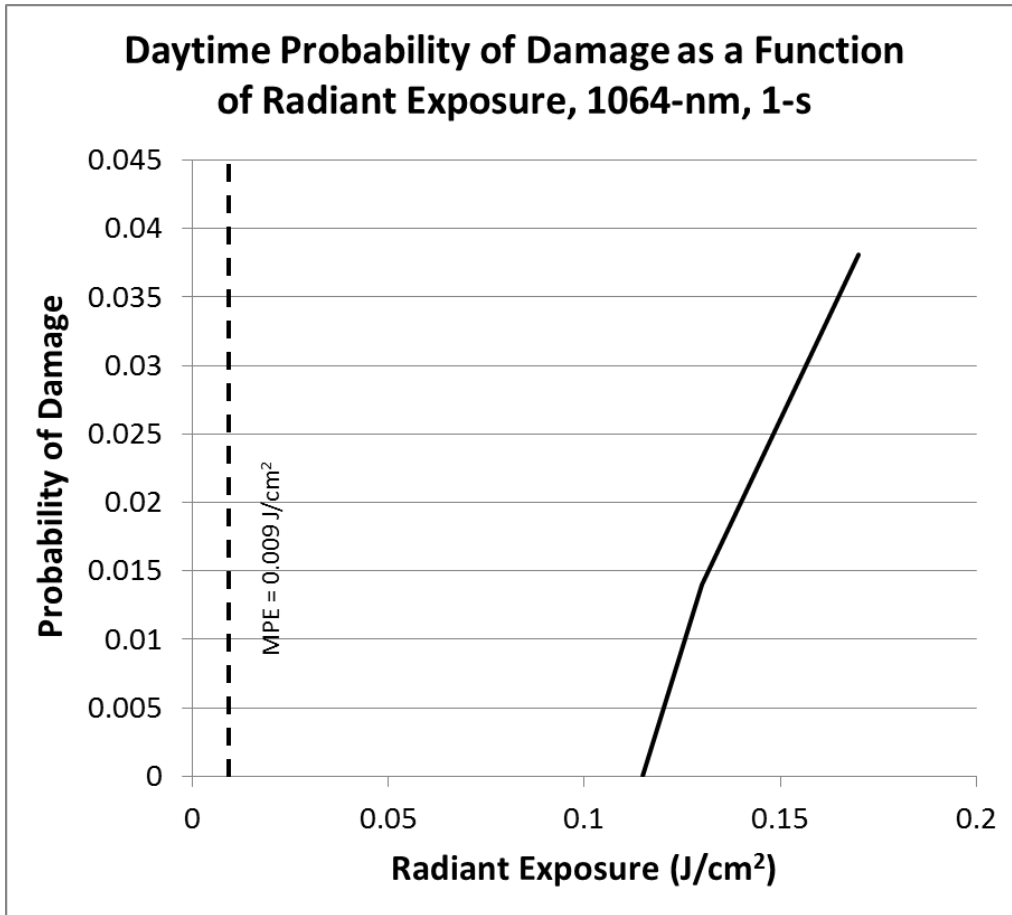


Figure 4.8 Plot depicting probability of damage as a function of radiant exposure for 0.3-cm pupil in daytime light conditions. Dashed line represents ANSI Z136.7-defined maximum permissible exposure (MPE) limit.

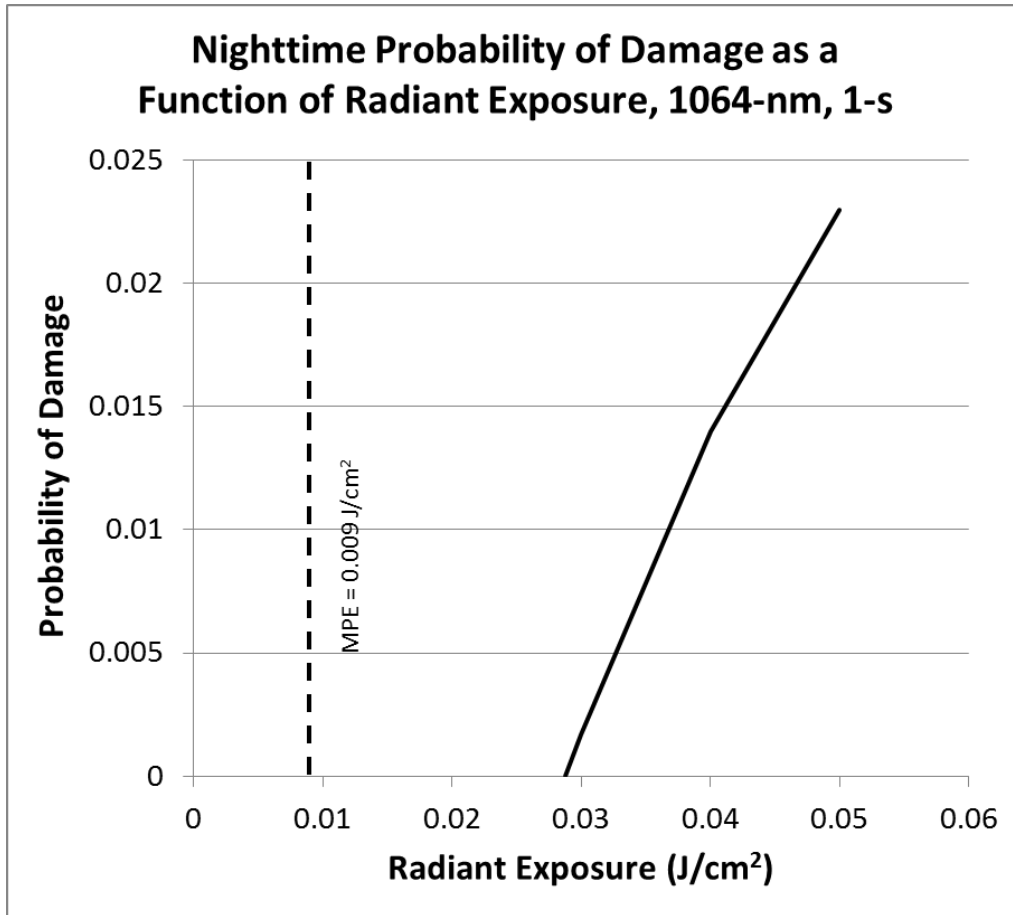


Figure 4.9 Plot depicting probability of damage as a function of radiant exposure for 0.6-cm pupil in nighttime light conditions. Dashed line represents ANSI Z136.7-defined maximum permissible exposure (MPE) limit.

5. *Conclusions, Recommendations, and Future Work*

This research effort establishes the foundation for the development of probabilistic models for laser damage to the human retina. The demand for these models stems from the need to prevent injuries by understanding the many influential factors on laser damage threshold research. Much of the variance in experimental results can be attributed to biological variance between subjects.

Chapter 3 describes the creation of a statistical eye model for estimating the biological variance of the human eye's refractive conditions and the effect it has on laser spot size and power density. The statistical eye model is used to create an input for a propagation model. The propagation model outputs are then used as an input for a thermal damage model. The final thermal model results are linked back to the initial statistical eye model to determine the initial biological distribution's influence on damage thresholds. The simulation results from Chapter 3 are the foundation for building empirical models such as a dose-response model used in applications such as risk assessment or collateral effects analysis tools.

The ratios of $\frac{ED_{84}}{ED_{50}}$ ranged between 1.48 and 2.68. These results varied from the theoretical values of 1.05 to 1.15 and experimental values of 1.5 and 1.7 reported by Sliney. However, this disagreement is expected for due to how the model is built. The scope of this study is to examine the full influence of an entire population distribution of refractive error. The only varying factor was focal geometry of the eye and its influence on spot size and power density. The full scope of refractive error naturally includes some values that would have excluded subjects from experiments. Therefore, the experimental and theoretical results can only properly be compared to a truncated refractive error distribution representing an experimentally feasible population, often having less than one diopter of refractive error. Further research may desire to resample the population of statistically generated eyes in order to model the controlled subject population with appropriate refractive error.

It is important to note that the effort described in Chapter 3 is based on assumptions of accurately representing the true human eye. The results of the population distributions of the eyes agree quite well with the data published in the original Rozema study. However, the published Rozema data did not include each parameter needed to estimate the retinal spot size from a laser beam in the ray trace model so some elements of the covariance structure had to be estimated using data collected from other studies. After the initial model was developed, I contacted Dr. Rozema to verify assumptions of normality in the data. He was extremely helpful and graciously permitted me to examine his complete data set that included some of the parameters that were needed by ray trace model. This effort creates a good approximation but a more complete data set collected with the intention of using the data explicitly to generate a population of eyes with all the parameters necessary to estimate spot size on the retina using a ray trace model is needed. A complete data set will eliminate the need to import factors into the covariance structure and allow for better population estimates for laser safety research. Nevertheless, this research effort provides a step by step approach to recreating a better model using the results of eye measurements from follow-on studies.

Chapter 4 details the development of a dose-response model for laser exposures from 10 to 1000 milliseconds and from 514 to 1064 nanometer wavelengths. The time and wavelength domains are sampled at appropriate intervals to estimate a damage threshold surface. The statistical eye model determines the probabilistic responses that are then linked to a time-dependent surface location. The surfaces are used interpolating the solution of the dose-response relationship to estimate the probability of damage for a given dose of laser energy. The model is also modified to solve the inverse problem to estimate the damage threshold for a user-defined probability of response.

It is noteworthy that the distribution of eyes generated by these models represent an uncorrected population. Depending on the application, this approach may

prove to need revision because a risk analysis effort to estimate damage from a dazzler system to civilians flying aircraft in the National Capitol Region must assume the pilots possess a corrected or uncorrected vision quality that would enable their flying. Truncating the distribution generated by the eye model or resampling a new distribution of operationally capable refractive error ranges would be an option to explore. Other risk analysis efforts such as those focusing on military applications where low-power laser systems target non-combatants or non-friendly forces must assume the true distribution of refractive errors in an operational setting. Truncation or resampling is also a viable solution in these cases.

Finally, the model developed in Chapter 3 may be used to generate the distribution of wavelengths not examined in this study. The dose-response model developed in Chapter 4 used this approach to sample wavelengths where anomalies in absorption characteristics created significant patterns in damage threshold. Examples of this occurs in the ranges of 500 to 650 and 800 to 1000 nanometers where absorption spikes. These and the original results of the model can also provide simulation inputs to examine time and pulse train dependencies. The results of these studies will enhance the domain of follow-on dose-response modeling efforts.

Expanding the body of knowledge associated with laser damage thresholds is critical for improving safety standards, developing new laser systems, and enhancing the capabilities of existing systems. Understanding the significance of the influences of biological variance and experimental errors and uncertainties will enable scientists to include only the biological variance component in the development of underlying probabilistic risk assessment models. Removing other sources of variance that are built into traditional analysis methods such as probit will shrink the spread of data, reduce unnecessarily large safety margins, and allow research in areas previously thought to be considered risky in nature. In the end, this research aims to help prevent unnecessary injury while simultaneously enabling a new premise for laser research and risk analysis.

Experiments will continue to be costly and the importance of modeling and simulation efforts will continue to be significant. Validation of these models is critical. The United States Air Force, the Department of Defense, and the international laser research community as a whole continue to develop higher quality models validated against experimental results. These models provide a means to reduce experimental costs while intelligently designed experiments may be used to validate the incremental modeling improvements.

I dedicate this research effort to the men and women of the directed energy community and hope that it serves as the foundation and roadmap for future retinal damage models as well as models for skin and cornea exposures.

Appendix A. Statistical Eye Model Code - FGenEyePop.m

```
function [f, d] = FGenEyePop(Lambda, CorneaSS, variates)

% Function that accepts a wavelength, beam radius at cornea, and
% desired population size and returns retinal beam diameter
% and associated empirical cumulative distribution function.

diffLimitedSpot = 0.0005;

% Initialize data from input files
S = load('CovMatrix.mat');
M = load('MeanVector.mat');
sd = load('StandDev.mat');
S = S.C;
Mu = M.Mu;
sd = sd.SD;
[m,n] = size(S);

% computer correlations from covariances
for i = 1:m
    for j = 1:n
        R(i,j) = S(i,j)/(sd(i)*sd(j));
    end
end

% compute eigenvectors/-values
[V,D] = eig(R);

% replace negative eigenvalues by zero
newD = max(D, 0);

% reconstruct correlation matrix
BB = V * newD * V';
```



```

% rescale correlation matrix
T      = 1 ./ sqrt(diag(BB));
TT     = T * T';
newR   = BB .* TT;

StDevs = diag(sd);

newS = StDevs*newR*StDevs;

X = mvnrnd(Mu, newS, variates);

%Vitreol Depth
X(:,18) = X(:,15) - X(:,14) - X(:,12) - X(:,13);

%Back/Front of lens
%Back
X(:,19) = X(:,15) - X(:,18);
%Front
X(:,20) = X(:,19) - X(:,12);

%Generate RV to assign to AL/CRC
X(:,21) = normrnd(3.03, 0.14, variates, 1); %distribution taken from
      nigerian study
X(:,23) = normrnd(1.21, 0.045, variates, 1); %distribution taken
      from Garner97

for i = 1:variates
    %Radius of Curvature Cornea - Anterior
    X(i,22) = X(i,15)./X(i,21);
    %Radius of Curvature Cornea - Anterior
    X(i,24) = X(i,22)./X(i,23);
end

```

```

%Send to ray trace function for spot size calculation for all
    variates
j = 1;
for i = 1:variates
    wr(i) = FEyeProp(Lambda, CorneaSS, X(i,14)/10, X(i, 12)/10, X(i
        ,18)/10, X(i,10)/10, X(i,11)/10, X(i,22)/10, X(i,24)/10, X(i
        ,13)/10);
    %Exclude spots less than diffraction limit
    %Another loop can be used to limit upper bound in cases where
    %refractive error is limited by the user.
    if wr(i) > diffLimitedSpot
        r(j) = wr(i);
        j = j + 1;
    end
end

end

[f, x] = ecdf(r);
d = 2*x;

```

Appendix B. Dose Response Model - Probability to Dose -

FProbToDose.m

```
function dose = FProbToDose(ExpDur, Lambda, CorneaSS, P_0, variates,
    rndReset)

% Function that uses midpoint search to find based on input dose
% and tolerance. Exposure parameters are:
%     ExpDur - exposure duration
%     Lambda - wavelength
%     CorneaSS - Spot Size at Cornea (radius, cm)

if rndReset == 1
    mtstream = RandStream('mt19937ar');
    RandStream.setGlobalStream(mtstream);
end

%% Prob Model Part
diffLimitedSpot = 0.0005;

Temp = load('BTECResults.mat');
T_Data = Temp.BTECResults;

for count = 1:length(T_Data(:,1))
    if T_Data(count,1) < 0.1
        counter10 = count;
    else if T_Data(count,1) < 1
        counter100 = count;
    end
end
end

ExpDur_in10 = T_Data(1:counter10,1);
Lambda_in10 = T_Data(1:counter10,2);
```

```

RetinaSS_in10 = T_Data(1:counter10,3);
Thresh_in10 = log10(T_Data(1:counter10,5));

ExpDur_in100 = T_Data(counter10+1:counter100,1);
Lambda_in100 = T_Data(counter10+1:counter100,2);
RetinaSS_in100 = T_Data(counter10+1:counter100,3);
Thresh_in100 = log10(T_Data(counter10+1:counter100,5));

ExpDur_in1000 = T_Data(counter100+1:count,1);
Lambda_in1000 = T_Data(counter100+1:count,2);
RetinaSS_in1000 = T_Data(counter100+1:count,3);
Thresh_in1000 = log10(T_Data(counter100+1:count,5));

%% Set up surface fits
[Lambda10, RetinaSS10, Thresh10] = prepareSurfaceData( Lambda_in10,
    RetinaSS_in10, Thresh_in10 );
[Lambda100, RetinaSS100, Thresh100] = prepareSurfaceData(
    Lambda_in100, RetinaSS_in100, Thresh_in100 );
[Lambda1000, RetinaSS1000, Thresh1000] = prepareSurfaceData(
    Lambda_in1000, RetinaSS_in1000, Thresh_in1000 );
ft = 'cubicinterp';
opts = fitoptions( ft );
opts.Normalize = 'on';

%% Fit models to data.
[surf10ms, gof] = fit( [Lambda10, RetinaSS10], Thresh10, ft, opts );
[surf100ms, gof] = fit( [Lambda100, RetinaSS100], Thresh100, ft,
    opts );
[surf1000ms, gof] = fit( [Lambda1000, RetinaSS1000], Thresh1000, ft,
    opts );

%% Eye Distribution Model Part

% Generate distribution from eye model to calculate probability from

```

```

%    spot size.

[f, d] = FGenEyePop(Lambda, CorneaSS, variates);
cdf = [f d];

i = 1;
while cdf(i, 1) < P_0
    i = i + 1;
end
spotsize = 10000*cdf(i,2);

T10 = 10^surf10ms(Lambda, spotsize);
T100 = 10^surf100ms(Lambda, spotsize);
T1000 = 10^surf1000ms(Lambda, spotsize);

DRTime = [0.01 0.1 1.0];
DRResults = [T10 T100 T1000];

% Interpolate time, dose grid
dose = pchip(DRTime, DRResults, ExpDur);

```

Appendix C. Dose Response Model - Dose to Probability -

FDoseToProb.m

```
function probability = FDoseToProb(dose, tol, ExpDur, Lambda,
    CorneaSS, variates)

% Function that uses midpoint search to find based on input dose
% and tolerance. Exposure parameters are:
%     dose - TIE at retina in microjoules
%     ExpDur - exposure duration
%     Lambda - wavelength
%     CorneaSS - Spot Size at Cornea (radius, cm)
% and user parameters are:
%     tol - tolerance (percent as a decimal)
%     variates - population size
% Random seed generator is fixed to reset to default after each run.

P = [0 1];

P_temp = FProbToDose(ExpDur, Lambda, CorneaSS, (P(1) + P(2))/2,
    variates, 1);

while dose < P_temp*(1-tol) || dose > P_temp*(1+tol)
    if dose < P_temp
        P(2) = (P(1) + P(2))/2;
    else
        P(1) = (P(1) + P(2))/2;
    end
    P_temp = FProbToDose(ExpDur, Lambda, CorneaSS, (P(1) + P(2))/2,
        variates, 1);
end

P_Out = P_temp;
probability = (P(1) + P(2))/2;
```

Appendix D. Ray Trace Approximation Code - FEyeProp.m

```
function [wr] = EyePropGeneral(Lambda, CorneaSS, t_antc, t_lens, tv,
    rlf, rlb, rcf, rcb, t_corn)

% Function to estimate spot size radius as a function of axial depth
% Thickness is measured in centimeters and each layer's
% cumulative thicknesses represent the entire axial depth.

% Lambda is wavelength in nanometers
% CorneaSS is radius of the beam at the cornea in centimeters

% ref index
n_corn = 1.3684 + 5/(Lambda-100);
n_aqua = 1.31618 + 10.36987/(Lambda-4.765);
n_lens = 1.3984 + 10/(Lambda-150);
n_vit = 1.30504 + 26.94137/(Lambda+349.150);

% Ray Matrices

% Propagation
T1 = [1 t_corn; 0 1];
T2 = [1 t_antc; 0 1];
T3 = [1 t_lens; 0 1];
T4 = [1 tv; 0 1];

% Interface
R1 = [1 0; (1-n_corn)/(rcf*n_corn) 1/n_corn];
R2 = [1 0; (n_corn-n_aqua)/(rcb*n_aqua) n_corn/n_aqua];
R3 = [1 0; (n_aqua-n_lens)/(rlf*n_lens) n_aqua/n_lens];
R4 = [1 0; (n_lens-n_vit)/(rlb*n_vit) n_lens/n_vit];

% Gaussian beam propagation through eye
```

% Rayleigh Range

```
Zr = (pi*CorneaSS^2)/(Lambda/1e7);  
i = sqrt(-1);  
q0 = i*Zr;  
w_corn = sqrt((-Lambda/1e7)/(pi*imag(1/q0)));
```

% Front surface of cornea refraction

```
Mc1 = (R1(1,1)*q0 + R1(1,2))/(R1(2,1)*q0 + R1(2,2));  
qc1 = 1/(real(1/Mc1) + i*imag(1/Mc1));
```

% Cornea propagation

```
Mc2 = (T1(1,1)*qc1 + T1(1,2))/(T1(2,1)*qc1 + T1(2,2));  
qc2 = 1/(real(1/Mc2) + i*imag(1/Mc2));
```

% Back surface of cornea

```
Ma1 = (R2(1,1)*qc2 + R2(1,2))/(R2(2,1)*qc2 + R2(2,2));  
qa1 = 1/(real(1/Ma1) + i*imag(1/Ma1));
```

% Spot size into aqueous

```
wa = sqrt((-Lambda/1e7)/(pi*n_corn*imag(1/qa1)));
```

% Aqueous propagation

```
Ma2 = (T2(1,1)*qa1 + T2(1,2))/(T2(2,1)*qa1 + T2(2,2));  
qa2 = 1/(real(1/Ma2) + i*imag(1/Ma2));
```

% Spot size into lens

```
wL1 = sqrt((-Lambda/1e7)/(pi*n_aqua*imag(1/qa2)));
```

% Front surface of lens

```
ML1 = (R3(1,1)*qa2 + R3(1,2))/(R3(2,1)*qa2 + R3(2,2));  
qL1 = 1/(real(1/ML1) + i*imag(1/ML1));
```

% Lens propagation


```

ML2 = (T3(1,1)*qL1 + T3(1,2))/(T3(2,1)*qL1 + T3(2,2));
qL2 = 1/(real(1/ML2) + i*imag(1/ML2));

% Back surface of lens
Mv1 = (R4(1,1)*qL2 + R4(1,2))/(R4(2,1)*qL2 + R4(2,2));
qv1 = 1/(real(1/Mv1) + i*imag(1/Mv1));

% Spot size out of lens
wL2 = sqrt((-Lambda/1e7)/(pi*n_lens*imag(1/qv1)));

% Vitreous propagation
Mv = (T4(1,1)*qv1 + T4(1,2))/(T4(2,1)*qv1 + T4(2,2));
qr = 1/(real(1/Mv) + i*imag(1/Mv));

% Spot size on retina
wr = sqrt((-Lambda/1e7)/(pi*n_vit*imag(1/qr)));

```

Appendix E. BTEC Config File - Main

#KeyValue main BTEC configuration (THIS MUST BE THE FIRST LINE IN THE FILE)

```
Dimensions                =      2
SimulationType            =    "Search"
AxialGridType             =      0
Nz                        =     500
zMin                     =      0
zMax                     =     0.1000
zInf                     =     0.1300
zStretchRatio            =      1
zMinBC                   =      3
zMaxBC                   =      0
RadialGridType           =      0
Nr                        =     500
rMax                     =     0.0700
rInf                     =     0.10
rStretchRatio            =      1
rMaxBC                   =      0
TotalSimTime             =     3.0
dtMax                    =     0.01
TissueBaseTemp           =     37
AmbientTemp              =     37
RelHumidity              =     1.0
AmbientRefIndex          =     1.0
LogDataFlag              =      0
LogInterval              =     50
ThermalLogInterval       =     -1
AxialLogInterval         =     -1
SourceLogInterval        =     -1
DamageLogInterval        =     -1
MaxPowerRatio            =     10.0
MinPowerRatio            =     0.1
ConvergeThresh           =     0.03
DamageThreshold          =     1.0
MaxTempThreshold         =    VALUE
InitialConditionsFlag    =      0
#InitialConditionsFile   =    "STRING"
Layer[0] = "layer.retina-vitreous.mainster.btec.1s-514nm.auto-gen.1"
Layer[1] = "layer.retina-rpe.mainsterx2.btec.1s-514nm.auto-gen.1"
Layer[2] = "layer.retina-choroid.mainster.btec.1s-514nm.auto-gen.1"
Layer[3] = "layer.retina-sclera.mainster.btec.1s-514nm.auto-gen.1"
```

```
StandardEmitter[0] = "beamTemplate.emitter.btec.1s-514nm.auto-gen.1"  
#Zscan[0] = "place_holder"  
Sensor[0] = "retina_damage.sensor.btec.1s-514nm.auto-gen.1"
```

Appendix F. BTEC Config File - Emitter

```
#KeyValue Standard Emitter configuration (THIS MUST BE THE FIRST LINE IN THE FILE)
#BaseEmitter Configuration Keys
EmitterType           = "LinAbsEmitter"
ProfileType           = 1
PeakPower              = 0.005
MinWavelength         = 514
FocusType             = 0
BeamDiameter          = 0.012
BeamDiameter2         = 0.0100
BeamWaistPosition     = 100.0
#BeamProfileFilename  = "STRING"
PulseType             = 1
PulseDuration         = 1.0
PulsePeriod           = 100.0
StartTime             = 0.0
StopTime              = 10000
TimeStepType          = 2
dtMinOn               = 5.0E-4
dtMinOff              = 1.0E-3
StretchOn             = 1.10
StretchOff            = 1.10
#Sensor[0]            = "place_holder"
#LinAbsEmitter Configuration Keys
# EmitterType = "LinAbsEmitter"
BeamDivergence        = 0.0015
```

Appendix G. BTEC Config File - Sensor

```
#SensorBase Configuration Keys
SensorType           = "TrapDamage"
PointSensor          = 0
LogInterval          = -1
LogPrecision         = 3
ScalarLogInterval    = 0
GradientLogInterval  = 0
ScalarMinLogInterval = -1
ScalarMaxLogInterval = -1
ScalarAvgLogInterval = -1
GradientMinLogInterval = 0
GradientMaxLogInterval = 0
GradientAvgLogInterval = 0
ExpandMinSensorRange = 1
TruncateMaxSensorRange = 0

#Sensor_2D Sepcific Configuration Keys
MinimumZaxisValue    = 0.0300
MaximumZaxisValue    = 0.0600
MinimumRaxisValue    = 0.0010
MaximumRaxisValue    = 0.0200
MaxThresholdValue    = 1
MaxThresholdError    = 0.03
MaxThresholdSearchAlg = "Midpoint"
```

Appendix H. BTEC Config File - Layer

```
#KeyValue layer configuration file
LayerType           = 11
Description          = "Retinal Pigment Epithelium"
Thickness            = 0.0012
Density              = 1.0
SpecificHeat         = 4.1868
Conductivity         = 0.00628
ConvHeatTransRate   = 0.0
Emissivity           = 1.0
BloodFlowRate       = 0.001
```

```
#Refractive index and dn/dt vs wavelength
RefractiveIndex[0]  = "0      1.33  1"
RefractiveIndex[1]  = "1000000 1.33  1"
```

```
#Scattering Anisotropy vs wavelength
Anisotropy[0]       = "0      0.8"
Anisotropy[1]       = "1000000 0.8"
```

```
#Scattering Coefficients vs wavelengt
Scattering[0]       = "0      0.0"
Scattering[1]       = "1000000 0.0"
```

```
#Reflectance
Reflectance[0]      = "400.0  0.080"
Reflectance[1]      = "500.0  0.070"
Reflectance[2]      = "514.5  0.070"
Reflectance[3]      = "520.8  0.070"
Reflectance[4]      = "600.0  0.070"
Reflectance[5]      = "647.1  0.075"
Reflectance[6]      = "694.3  0.079"
Reflectance[7]      = "700.0  0.080"
Reflectance[8]      = "800.0  0.095"
Reflectance[9]      = "900.0  0.144"
Reflectance[10]     = "1000.0 0.210"
Reflectance[11]     = "1060.0 0.252"
Reflectance[12]     = "1064.0 0.255"
Reflectance[13]     = "1100.0 0.280"
Reflectance[14]     = "1200.0 0.260"
Reflectance[15]     = "1400.0 0.260"
```

```

Temp[0] = 0.0      # DBL: temperature for rate coefficients
  A[0] = 3.1e99   # DBL: A rate coef. [1/s]
  Ea[0] = 6.28e5  # DBL: Ea rate coef. [J/mole]
Temp[1] = 99999   # DBL: temperature for rate coefficients
  A[1] = 3.1e99   # DBL: A rate coef. [1/s]
  Ea[1] = 6.28e5  # DBL: Ea rate coef. [J/mole]

```

```
#Absorption
```

```

# M.A. Mainster, T.J. White, J.H. Tips, P.W. Wilson
# "Retinal-Temperature Increases Produced by Intense Light Sources"
# Journal of the Optical Society of America 60(2), 264-271, (1970).

```

```

Absorption[0] = "0      0"
Absorption[1] = "399    0"
Absorption[2] = "400    6000"
Absorption[3] = "420    2800"
Absorption[4] = "440    2000"
Absorption[5] = "460    1800"
Absorption[6] = "480    1800"
Absorption[7] = "500    1840"
Absorption[8] = "520    1680"
Absorption[9] = "540    1400"
Absorption[10] = "560    1200"
Absorption[11] = "580    1040"
Absorption[12] = "600    960"
Absorption[13] = "620    880"
Absorption[14] = "640    800"
Absorption[15] = "660    760"
Absorption[16] = "680    720"
Absorption[17] = "700    640"
Absorption[18] = "720    600"
Absorption[19] = "740    560"
Absorption[20] = "760    520"
Absorption[21] = "780    400"
Absorption[22] = "800    280"
Absorption[23] = "820    260"
Absorption[24] = "840    250"
Absorption[25] = "860    240"
Absorption[26] = "880    210"
Absorption[27] = "900    200"
Absorption[28] = "920    196"
Absorption[29] = "940    152"
Absorption[30] = "960    144"

```

Absorption[31]	=	"980	168"
Absorption[32]	=	"1000	176"
Absorption[33]	=	"1020	176"
Absorption[34]	=	"1040	164"
Absorption[35]	=	"1060	152"
Absorption[36]	=	"1080	144"
Absorption[37]	=	"1100	140"

Appendix I. Rozema Statistical Eye Model Data

Table I.1 contains the mean values and covariance data taken from the human eye study.

Table I.1 Table of eye data taken from Rozema study.

	Covariance Matrix																
Age	147.8	-0.322	-2.81	-0.324	-0.825	-0.181	-0.069	-0.139	1.271	-8.971	1.555	5.067	0.017	2.554	-4.691	-6.375	2.174
Anterior Keratometry (D) - K_{A,M}	-0.322	1.836	0.127	-0.017	0.01	-0.273	-0.036	0.006	-0.108	-0.072	0.089	-0.043	-0.002	0.031	-0.581	-0.289	0.065
K_{A,J0}	-2.81	0.127	0.077	0.004	0.014	-0.021	-0.012	0.002		-0.033	-0.021	0.024	-0.001	-0.016	-0.065	-0.056	0.06
K_{A,J45}	-0.324	-0.017	0.004	0.051	0.001	0.004	-0.001	-0.004	-0.009	0.066	0.009	-0.022	-0.001	0.005	-0.019	0.038	0.101
Ant Corneal Eccentricity	-0.825	0.01	0.014	0.001	0.03	-0.001	-0.001		0.003	0.033	-0.021	-0.031		0.004	0.035	0.022	0.01
Posterior Keratometry (D) - K_{P,M}	-0.181	-0.273	-0.021	0.004	-0.001	0.05	0.007	-0.002	0.008	0.03	-0.03	0.008	-0.001	0.006	0.107	0.08	-0.026
K_{P,J0}	-0.069	-0.036	-0.012	-0.001	-0.001	0.007	0.005		-0.001		-0.003	0.002		0.004	0.021	0.017	-0.02
K_{P,J45}	-0.139	0.006	0.002	-0.004		-0.002		0.003		-0.009	0.003	-0.002		-0.001	-0.005	-0.004	-0.01
Post Corneal Eccentricity	1.271	-0.108		-0.009	0.003	0.008	-0.001		0.077	-0.196	0.068	0.063		-0.041	-0.033	-0.075	0.113
Radius Curvature - Lens Ant (mm)	-8.971	-0.072	-0.033	0.066	0.033	0.03		-0.009	-0.196	1.924	-0.616	-0.376	-0.011	0.316	0.311		-1.136
Radius Curvature - Lens Post (mm)	1.555	0.089	-0.021	0.009	-0.021	-0.03	-0.003	0.003	0.068	-0.616	0.712	0.098	-0.001	-0.05	-0.172		0.924
Lens Thickness (mm)	5.067	-0.043	0.024	-0.022	-0.031	0.008	0.002	-0.002	0.063	-0.376	0.098	0.191		-0.091	-0.008		0.185
Cornea Thickness (mm)	0.017	-0.002	-0.001	-0.001		-0.001				-0.011	-0.001		0.001	-0.002	0.001	-0.002	-0.012
Anterior Chamber Depth (mm)	2.554	0.031	-0.016	0.005	0.004	0.006	0.004	-0.001	-0.041	0.316	-0.05	-0.091	-0.002	0.143	0.239	0.264	-0.287
Axial Length (mm)	-4.691	-0.581	-0.065	-0.019	0.035	0.107	0.021	-0.005	-0.033	0.311	-0.172	-0.008	0.001	0.239	1.233	0.653	-1.12
Pupil Size (Scotopic)	-6.375	-0.289	-0.056	0.038	0.022	0.08	0.017	-0.004	-0.075				-0.002	0.264	0.653	1.237	-0.75
Lens Power (D)	2.174	0.065	0.06	0.101	0.01	-0.026	-0.02	-0.01	0.113	-1.136	0.924	0.185	-0.012	-0.287	-1.12	-0.75	4.561
Mean Value	39.88	43.29	0.297	0.06	0.403	-6.265	-0.166	-0.003	0.151	10.43	-6.864	4.07	0.545	2.87	23.67	6.505	22.99

Appendix J. Quad Chart



PROBABILISTIC MODEL FOR LASER DAMAGE TO THE HUMAN RETINA



Introduction

- Laser damage thresholds are reported as a distribution based on convolution of experimental error, variance, and uncertainty
- Modeling efforts supporting eye safety applications must quantify contribution from biological variance
- Using a statistical model eye developed in this research, biological distributions are sampled to determine contribution of population variance

Capt David Wooddell
 Advisor: Dr. Raymond Hill
 Reader: Dr. Chritine Schubert-Kabban
 Department of Operational Sciences (ENS)
 Air Force Institute of Technology

Sponsoring Organization
 711 HPW/RHDO
 Air Force Research Laboratory
 Fort Sam Houston, Texas

Significance

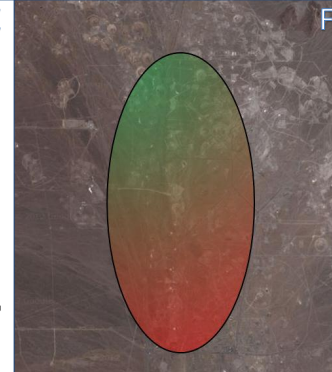
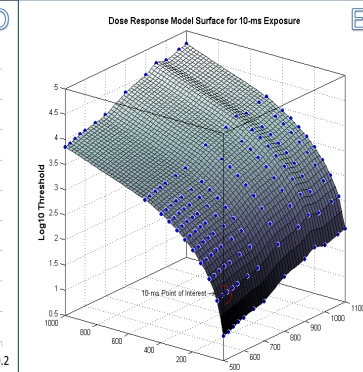
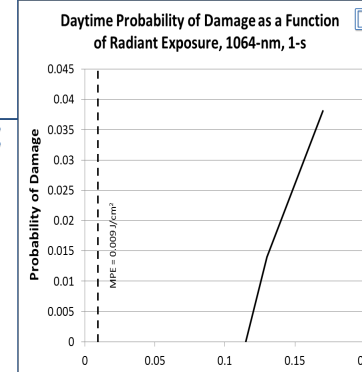
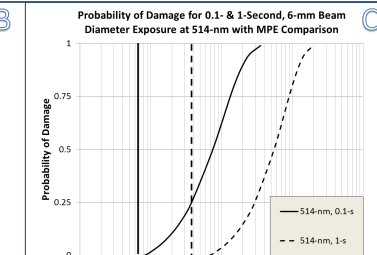
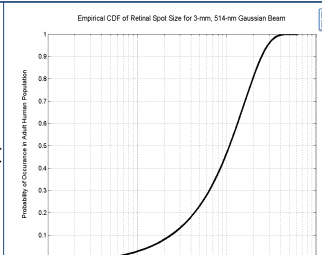
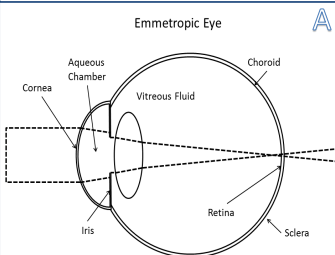
- First-ever probabilistic model to estimate damage threshold based on biological variance
- Developed statistical eye model to predict power density at the retina for thermal damage threshold simulation
- Provides foundation for \$2M/yr risk assessment and decision support tools efforts

Algorithm

- User input for laser beam parameters: λ – wavelength, t – exposure duration, r – input beam radius
- Generate eye population of size n (A) for Gaussian beam ray trace propagator using λ, r to estimate spot sizes distribution (r')
- Sample empirical distribution of r' for p^{th} -percentile (B)
- Export results to BTEC Thermal Model to estimate damage threshold, Φ , for λ, t, r' , using time-temperature profile integration in Arrhenius Model
- Report distribution of population damage thresholds using $\Phi(p)$ - provides foundation for other probabilistic models for risk assessment, decision support tools, trade-space analysis, and safety standards development (C)

Results

- Biological variance found to be wavelength and time dependent
- Statistical model eye results improved due to spectral decomposition method for dealing with missing data
- Provides foundation for future probabilistic applications for retinal damage such as trade-space analyses applications (D), dose-response modeling (E), probabilistic risk assessment and decision-support tools (F)
- Easily adaptable to other new sources of data, skin damage studies



Bibliography

1. American National Standard ANSI Z136.1 *Safe Use of Lasers*. Laser Institute of America, 2007.
2. Ahmed, E., D. Wooddell, and R. Thomas. *A probabilistic 1064 nm Dose Response Model*. Technical Report AFRL-RH-BR-TR-2008-0030, Air Force Research Lab, Brooks City-Base, Texas, 2008.
3. Airborne Laser System Program Office. *Contact at the Speed of Light - The Lasers that Make Up the Airborne Laser System*.
4. Clark, C.D., M. Denton, and R. Thomas. “Mathematical Model that Describes the Transition from Thermal to Photochemical Damage in Retinal Pigment Epithelial Cell Culture”, *JBO*, 16(2), February 2011.
5. Del Priore, L., Y. Kuo, and T. Tezel. “Age-Related Changes in Human RPE Cell Density and Apoptosis Proportion in Situ”, *IOVS*, 43(10):3312–3318, October 2002.
6. DeMarco, S., G. Lazzi, W. Liu, J. Weiland, and M. Humayun. “Computed SAR and Thermal Elevation in a 0.25-mm 2-D Model of the Human Eye and Head in Response to an Implanted Retinal Stimulator - Part I: Models and Methods”, *IEEE Transactions on Antennas and Propagation*, 51(9):2274–2285, September 2003.
7. DoD. *Department of Defense Fiscal Year 2012 Budget Estimates for Defense Advanced Research Projects Agency*. Technical report, Defense Advanced Research Projects Agency, February 2011.
8. Dunaway, D. and I. Berger. “Worldwide Distribution of Visual Refractive Errors and What to Expect at a Particular Location”. *Presentation to International Society for Geographic and Epidemiologic Ophthalmology*.
9. Finney, D. J. *Probit Analysis 3rd Edition*. Cambridge University Press, 1971.
10. Fritsch, F. and R. Carlson. “Monotone Piecewise Cubic Interpolation”, *SIAM Journal on Numerical Analysis*, 17:238–246, 1980.
11. Garner, L., H. Owens, M. Yap, M. Frith, and R. Kinnear. “Radius of curvature of the posterior surface of the cornea”, *Optom Vis Sci*, 74(7):496–8, Jul 1997.
12. General, Inspector. *Marine Corps Response to Nonlethal Laser Dazzler Urgent Request*. Technical report, United States Department of Defense, February 2011.
13. Hariri, S., A. Moayed, and A. Dracopoulos. “Limiting factors to the OCT axial resolution for in-vivo imaging of human and rodent retina in the 1060nm wavelength range”, *Optics Express*, 17(26), 2009.

14. Higham, N. "Computing the Nearest Correlation Matrix-a Problem from Finance", *IMA J Numer Anal*, 22(3):329–343, 2002.
15. Irvin, L. *BTEC Thermal Model*. Technical Report AFRL-RH-BR-TR-2008-0006, Air Force Research Laboratory, Brooks City-Base, Texas, 2008.
16. Iyamu, E., J. Iyamu, and C. Obiakor. "The Role of Axial Length-Corneal Radius of Curvature Ratio in Refractive State Categorization in a Nigerian Population", *International Scholarly Research Network Ophthalmology*, May 2011.
17. Kahaner, D., C. Moler, and S. Nash. *Numerical Methods and Software*. Prentice-Hall, 1989.
18. Keller, J. "NORAD to test aircraft laser warning system this week around Washington, D.C., area", *Military and Aerospace Electronics*, May 2009.
19. Kempen, J. "The Prevalence of Refractive Errors Among Adults in the United States, Western Europe, and Australia", *Arch Ophthalmol*, 122:495–505, 2004.
20. Kennedy, P. and J. Zuclich. "Laser induced retinal damage thresholds for annular retinal beam profiles". S. Jacques and W. Roach (editors), *Laser Interaction with Tissue and Cells XV*, volume 5319. SPIE, 2004.
21. Lund, D. "Variation of laser-induced retinal injury thresholds with retinal irradiated area: 0.1-s duration, 514-nm exposures", *J. Biomed. Opt*, 12, 2007.
22. Maher, E. *Transmission and Absorption Coefficients for Ocular Media of the Rhesus Monkey*. Technical report, USAF School of Aerospace Medicine, Brooks Air Force Base, Texas, 1978.
23. Niesink, R. and A. Musch. *Toxicology: Principles and Applications*. CRC Press, 1996.
24. Ogle, K. "Depth of Focus of the Human Eye", *J. Opt. Soc. Am.*, 49(3):273–279, 1959.
25. Ohab, J. "Laser Creates Universal Stop Sign", *Armed with Science*, 2010.
26. Oliver, J. "Visible Lesion Laser Thresholds in Cynomolgus (*Macaca fascicularis*) Retina with a 1064-nm, 12-ns Pulsed Laser", *Proc. of SPIE*, 6435, 2007.
27. Rockwell, B., D. Hammer, and P. Kennedy. "Retinal Spot Size with Wavelength". *Proceedings of SPIE, Vol. 2975*, volume 2975.
28. Rongjia, C., C. Renyuan, and L. Mengchang. "Injury Threshold of Human Eye by Pulsed YAG Laser Beams, Pathological Observation", *Chinese Journal of Lasers*, 615–617, 1985.
29. Rozema, J., D. Atchison, and M. Tassignon. "Statistical Eye Model for Normal Eyes", *IOVS*, 10-6705, March 2011.

30. Schmitt, J. M. “Optical Coherence Tomography (OCT): A Review”, *IEEE Journal of Selected Topics in Quantum Electronics*, 5(4), July 1999.
31. Schulmeister, K. “Modeling of Uncertainty Associated with Dose-Response Curves as Applied for Probabilistic Risk Assessment in Laser Safety”, *Proceedings of SPIE*, 4246:155–172, 2001.
32. Schulmeister, K., G. Sonneck, and F. Rattay. “A Probabilistic Risk Analysis Model for Receiving Laser Eye Injury from Space Based Lasers”, *Joint ESA-NASA Space Flight Safety Conference*, 2002.
33. Sliney, D., J. Mellerio, and K. Schulmeister. “What is the Meaning of Thresholds in Laser Injury Experiments?”, *Health Physics*, 82(3):335–47, March 2002.
34. Sliney, David H. “Implications of Using ED-50 and Probit Analysis in Comparing Retinal Injury Threshold Data”, , 2001.
35. Smith, P. *Final Report for Vision Science and Personnel Susceptibility Task Order 14*. Technical report, Air Force Research Laboratory, Brooks City-Base, Texas, 2009.
36. Townes, C. *A Century of Nature: Twenty-One Discoveries that Changed Science and the World*. The University of Chicago Press, 2003.
37. Vassiliadis, A. *Investigations of Laser Damage to Ocular Tissues*. Technical Report AFAL-TR-67-170, Stanford Research Institute, March 1967.
38. Wang, J. and C. Liu. “Generating Multivariate Mixture of Normal Distributions Using a Modified Cholesky Decomposition”. *Proceedings of the 2006 Winter Simulation Conference*, 342–347.
39. Wang, Y., J. Nelson, and Z. Chen. “Optimal wavelength for ultrahigh-resolution optical coherence tomography”, *Optics Express*, 11(12), June 2003.
40. Wenzel, A., K. Fuld, and J. Stringham. “Light Exposure and Macular Pigment Optical Density”, *Invest. Ophthalmol. Vis. Sci.*, 44(1):306–309, January 2003.
41. Wolbarsht, M. L. and D. H. Sliney. “1991, 1992, Historical Development of the ANSI laser safety standard”, *Journal of Laser Applications*, 1992.
42. Wooddell, D., R. Hill, and C. Schubert-Kabban. “An Analysis of the Influences of Biological Variance, Measurement Error, and Uncertainty on Retinal Photothermal Damage Threshold Studies (Est Pub Date Mar 2012)”. *Proceedings of SPIE 2012*. SPIE.
43. Zuclich, J. and D. Lund. “Laser-induced retinal damage threshold as a function of retinal image size”. *Ophthalmic Technologies IX*, volume 3591, 335–343. 1999.

Vita

David Alan Wooddell, Jr., was born in Schenectady, NY, 1975, but spent most of his life in East Texas. He graduated in 1993 from Robert E. Lee High School in Tyler, Texas. In January 1996, he enlisted in the United States Air Force where he served as a Far East Cryptological Linguist. He served 8 1/2 years before being selected to the Airman's Education and Commissioning Program at the University of Maryland. Upon completion of his Bachelor of Science Degree in Mathematics, he commissioned as a Second Lieutenant in the United States Air Force. His first duty assignment was at the Air Force Research Laboratory's Directed Energy Bio-effects Division in San Antonio, Texas, where he led the Optical Radiation Branch's Modeling and Simulation Integrated Product Team. His work included laser-tissue interaction modeling, software and model integration, distributed simulations model development, probabilistic dose response modeling, and visual performance modeling. He received two Air Force Achievement Medals and the Air Force's Scientist Team Award of 2009. He currently resides in Beavercreek, Ohio, with his wife and two children.

Permanent address: 11520 County Road 137
Flint, Texas 75762

REPORT DOCUMENTATION PAGE

Form Approved
OMB No. 0704-0188

Public reporting burden for this collection of information is estimated to average 1 hour per response, including the time for reviewing instructions, searching existing data sources, gathering and maintaining the data needed, and completing and reviewing this collection of information. Send comments regarding this burden estimate or any other aspect of this collection of information, including suggestions for reducing this burden to Department of Defense, Washington Headquarters Services, Directorate for Information Operations and Reports (0704-0188), 1215 Jefferson Davis Highway, Suite 1204, Arlington, VA 22202-4302. Respondents should be aware that notwithstanding any other provision of law, no person shall be subject to any penalty for failing to comply with a collection of information if it does not display a currently valid OMB control number. **PLEASE DO NOT RETURN YOUR FORM TO THE ABOVE ADDRESS.**

1. REPORT DATE (DD-MM-YYYY) 22-03-2012		2. REPORT TYPE MASTER'S THESIS		3. DATES COVERED (From - To) MAR 2011 - MAR 2012	
4. TITLE AND SUBTITLE Probabilistic Model for Laser Damage to the Human Retina				5a. CONTRACT NUMBER	
				5b. GRANT NUMBER	
				5c. PROGRAM ELEMENT NUMBER	
6. AUTHOR(S) DAVID A. WOODDELL, JR., CAPT, USAF				5d. PROJECT NUMBER	
				5e. TASK NUMBER	
				5f. WORK UNIT NUMBER	
7. PERFORMING ORGANIZATION NAME(S) AND ADDRESS(ES) Air Force Institute of Technology Graduate School of Engineering and Management (AFIT/EN) 2950 Hobson Street, Building 642 WPAFB OH 45433-7765				8. PERFORMING ORGANIZATION REPORT NUMBER AFIT-OR-MS-ENS-12-30	
9. SPONSORING / MONITORING AGENCY NAME(S) AND ADDRESS(ES) 711 HPW/RDHO ATTN: Dr. Robert Thomas 4141 Petroleum Road Fort Sam Houston, TX 78234-2644				10. SPONSOR/MONITOR'S ACRONYM(S)	
				11. SPONSOR/MONITOR'S REPORT NUMBER(S)	
12. DISTRIBUTION / AVAILABILITY STATEMENT DISTRIBUTION STATEMENT A: APPROVED FOR PUBLIC RELEASE; DISTRIBUTION UNLIMITED					
13. SUPPLEMENTARY NOTES					
14. ABSTRACT The proliferation of laser systems in the 21st-century is fueled by an increasing demand and comprehension of the capabilities they provide. Understanding how lasers interact with media during propagation is a premiere field of physics. The subject area known as laser bioeffects explores laser interactions with biological cells, tissues, organs, and bodies. This research includes laser applications used in medicine, establishes safe exposure limits for industry and academia, and generally studies the many effects of laser light on living creatures. The bioeffects community relies heavily on deterministic modeling and simulation tools to support experimental research into damage thresholds and laser effects. However, recent laser applications require a probabilistic approach to support risk management and analyses methodologies. Some probabilistic models exist but their assumptions are largely biased due to sampling and reporting techniques. This research focuses on building the first-ever population based probabilistic model for retinal damage using a statistical model of the optical properties and dimensions of the human eye. Simulated population distributions are used as input to propagation and thermal damage model for analysis. The results of this research are intended to provide a foundation for future probabilistic models and applications.					
15. SUBJECT TERMS Dose-response, laser damage, probit analysis, ED50, biological variance, retinal damage threshold, statistical eye model, BTEC					
16. SECURITY CLASSIFICATION OF:			17. LIMITATION OF ABSTRACT UU	18. NUMBER OF PAGES 111	19a. NAME OF RESPONSIBLE PERSON Raymond R. Hill, Ph.D.
a. REPORT U	b. ABSTRACT U	c. THIS PAGE U			19b. TELEPHONE NUMBER (include area code) (937) 255-6565 raymond.hill@afit.edu